HHS Public Access

Author manuscript

Nature. Author manuscript; available in PMC 2020 September 18.

Published in final edited form as:

Nature. 2020 March ; 579(7800): 586–591. doi:10.1038/s41586-020-2101-7.

Dietary fructose feeds hepatic lipogenesis via microbiota-derived acetate

Steven Zhao[1,2,6,*], **Cholsoon Jang**[8,*], **Joyce Liu**[1,2,7], **Kahealani Uehara**[3,4,7], **Michael Gilbert**[1,2,7], **Luke Izzo**[1,2,6], **Xianfeng Zeng**[8], **Sophie Trefely**[1,2,9], **Sully Fernandez**[1,2], **Alessandro Carrer**[1,2,11], **Katelyn D. Miller**[10], **Zachary T. Schug**[10], **Nathaniel W. Snyder**[9], **Terence P. Gade**[1,5], **Paul M. Titchenell**[3,4], **Joshua D. Rabinowitz**[8], **Kathryn E. Wellen**[1,2,4,‡]

[1]Department of Cancer Biology, University of Pennsylvania Perelman School of Medicine, Philadelphia, PA, USA 19104

[2]Abramson Family Cancer Research Institute, University of Pennsylvania Perelman School of Medicine, Philadelphia, PA, USA 19104

[3]Department of Physiology, University of Pennsylvania Perelman School of Medicine, Philadelphia, PA, USA 19104

[4]Institute of Diabetes, Obesity and Metabolism, University of Pennsylvania Perelman School of Medicine, Philadelphia, PA, USA 19104

[5]Department of Radiology, University of Pennsylvania Perelman School of Medicine, Philadelphia, PA, USA 19104

[6]Cell & Molecular Biology Graduate Group, University of Pennsylvania Perelman School of Medicine, Philadelphia, PA, USA 19104

[7]Biochemistry & Molecular Biophysics Graduate Group, University of Pennsylvania Perelman School of Medicine, Philadelphia, PA, USA 19104

[8]Department of Chemistry and Lewis-Sigler Institute for Integrative Genomics, Princeton University, Princeton, NJ, USA 08544

[9]A.J. Drexel Autism Institute, Drexel University, Philadelphia, PA, USA 19104

[10]Molecular and Cellular Oncogenesis, Wistar Institute, Philadelphia, PA, USA 19104

‡Correspondence should be addressed to K.E.W. (wellenk@upenn.edu).

*Co-first author

Author Contributions:

The project was conceptualized and designed by S.Z., C.J. and K.E.W. K.E.W. and J.D.R. guided the study. S.Z. generated LAKO mice and performed majority of animal experiments, with help from J.L., S.F., A.C. and K.D.M. C.J. performed animal experiments and the majority of LC-MS analyses with help from X.Z. for LC-MS analysis of SCFA species. S.T. and N.W.S. performed LC-MS analysis of acyl-CoA species. K.U. isolated and performed experiments on primary hepatocytes. J.L., M.G. and L.I. performed experiments. P.M.T., Z.T.S. and T.P.G. provided guidance into study design. S.Z. prepared figures with input from C.J., J.D.R., and K.E.W. S.Z., C.J., and K.E.W. wrote and edited the manuscript, with input from J.D.R. All authors read and provided feedback on manuscript and figures.

J.D.R. is a consultant to Pfizer and to Colorado Research Partners. All other authors declare no conflicts of interest.

Data Availability: All data generated or analysed during this study are included in this published article (and its supplementary information files).

[11]Present address: Veneto Institute of Molecular Medicine (VIMM), Via Orus 2, 35129 Padua, Italy

Abstract

Fructose consumption has risen dramatically in recent decades due to use of sucrose and high fructose corn syrup in beverages and processed foods[1], contributing to rising rates of obesity and non-alcoholic fatty liver disease (NAFLD)[2–4]. Fructose intake triggers hepatic *de novo* lipogenesis (DNL)[4–6], which is initiated from acetyl-CoA. ATP-citrate lyase (ACLY) cleaves cytosolic citrate to generate acetyl-CoA and is upregulated upon carbohydrate consumption[7]. Ongoing clinical trials are pursuing ACLY inhibition for treatment of metabolic diseases[8]. Nevertheless, the route from dietary fructose to hepatic acetyl-CoA and lipids remains unproven. Here we show, using *in vivo* isotope tracing, that liver-specific deletion of *Acly* fails to suppress fructose-induced DNL in mice. Dietary fructose is converted by the gut microbiome into acetate[9], which supplies lipogenic acetyl-CoA independently of ACLY[10]. Depletion of the microbiome or silencing of hepatic ACSS2, which generates acetyl-CoA from acetate, potently suppresses conversion of a fructose bolus into hepatic acetyl-CoA and fatty acids, bypassing ACLY. When fructose is consumed more gradually to facilitate its absorption in the small intestine, both citrate cleavage and microbial acetate contribute to lipogenesis. The DNL transcriptional program, on the other hand, is activated in response to fructose in a manner independent of acetyl-CoA metabolism. These data reveal a two-pronged mechanism regulating hepatic DNL, in which fructolysis within hepatocytes provides a signal to promote DNL gene expression, while microbial acetate generation feeds lipogenic acetyl-CoA pools.

Fructose-driven DNL is ACLY-independent

Since ACLY links carbohydrate and lipid metabolism (Extended Data Fig. 1a), we hypothesized that genetic deletion of *Acly* in hepatocytes would protect mice against fructose-induced lipid accumulation. While whole body *Acly* knockout is embryonic lethal[11], liver-specific *Acly* knockout (LAKO) mice were grossly indistinguishable from wild-type (WT) littermate controls, with similar body weights and organ sizes between genotypes on either standard chow or a high-fructose (60%) diet (HFrD) (Extended Data Fig. 1b–c). Fructose consumption triggered mild hepatic lipid accumulation, without fibrosis or excess glycogen accumulation, in both WT and LAKO mice (Fig. 1a, Extended Data Fig. 1d–e). Metabolomic and lipidomic analyses revealed striking diet-dependent changes, and relatively modest genotype-dependent differences (Extended Data Fig. 2a–b, 3a–c, Supplementary Tables 1 and 2). Consistent with loss of ACLY activity, accumulation of citrate and its downstream metabolite aconitate was observed in LAKO livers (Extended Data Fig. 2c). These data demonstrate that ACLY deficiency, surprisingly, neither dramatically impacts global hepatic metabolite levels nor prevents fructose-induced accumulation of triglyceride.

To further investigate the role of hepatic ACLY in fructose-induced steatosis without altering the overall diet, we fed mice standard chow diets with either normal drinking water (H_2O) or drinking water containing a 1:1 mixture of fructose and glucose (15% each, Fruc:Gluc) (Extended Data Fig. 4a–c). Similar to HFrD, WT and LAKO mice drinking Fruc:Gluc for 4 weeks developed mild hepatic steatosis (Extended Data Fig. 4d). Moreover, deuterated water

(D_2O) tracing revealed that Fruc:Gluc consumption increases hepatic DNL to a similar extent in WT and LAKO mice (Fig. 1b). Thus, deletion of *Acly* from liver does not prevent DNL in response to fructose consumption.

Given this unexpected result, we directly tested the impact of ACLY deficiency on fructose conversion into nascent fatty acids. WT and LAKO mice were gavaged with 1:1 fructose:glucose, with either glucose or fructose ^{13}C-labeled (Extended Data Fig. 4e). Strikingly, fructose carbons were incorporated into fatty acids in LAKO and WT mice to a similar extent, while glucose carbons were barely used (Fig. 1c, Extended Data Fig. 4f). These data indicate that, in contrast with existing models of fructose metabolism, the use of fructose carbons for hepatic DNL does not require ACLY.

Microbial acetate feeds lipogenesis

We next investigated the mechanisms of how fructose carbons are used for fatty acid synthesis in an ACLY-independent manner. It has been previously shown that the hepatic DNL program is activated in response to carbohydrate consumption by ChREBP[12,13]. Upon chronic high fructose consumption, livers of both WT and LAKO mice upregulated the highly active ChREBP-β isoform[14], along with lipogenic genes (*Acaca* and *Fasn*) and other ChREBP target genes, aldolase B (*AldoB*), and ketohexokinase (*Khk*)[15] (Extended Data Fig. 5a–b). WT mice also exhibited upregulation of *Acly* on HFrD (Extended Data Fig. 5a). The induction of the DNL program was also robust at the protein level, with residual ACLY protein in fructose-fed LAKO livers in cells other than hepatocytes (Fig. 1d, Extended Data Fig. 5c–d). Acyl-CoA synthetase short chain family member 2 (ACSS2), which converts acetate into acetyl-CoA, was notably upregulated in fructose-consuming LAKO mice (Fig. 1d, Extended Data Fig. 5b–c). Moreover, the *Acss2* genomic locus showed increased histone H3K27 acetylation after Fruc:Gluc drinking (Extended Data Fig. 5e). ChREBP binding to the *Acss2* locus was identified in a published ChIP-Seq dataset[16] (Extended Data Fig. 5f). *Acss2* is also a target of SREBP transcription factors, which are activated in response to fructose consumption[17–19]. These data suggest that ACSS2 is a component of the hepatic response to fructose consumption.

Since acetate conversion to acetyl-CoA by ACSS2 can support *de novo* lipogenesis in the absence of ACLY[10], we hypothesized that acetate might be an important source of acetyl-CoA for DNL in the context of fructose feeding (Fig. 2a). Acetate can be generated within mammalian cells through several mechanisms[20–22], prompting us to investigate if fructose is converted to acetate in a cell autonomous manner in hepatocytes. Incubation of murine hepatocytes with 25 mM ^{13}C-fructose labeled fructolytic intermediates (Fig. 2b), but only minimally labeled acetyl-CoA and malonyl-CoA, the core DNL substrates (Fig. 2c). In contrast, 1 mM ^{13}C-acetate was readily used for synthesis of acetyl-CoA and malonyl-CoA, as well as HMG-CoA, an intermediate in the mevalonate pathway downstream of acetyl-CoA (Fig. 2c). Therefore, even when ACLY is intact, exogenous acetate directly feeds into lipogenic acetyl-CoA pools in hepatocytes.

We thus investigated the possibility that fructose is converted to acetate prior to reaching the liver to feed hepatic DNL by performing a ^{13}C-fructose tracing time course in mice. Orally

administered ^{13}C-fructose labeled fructose-1-phosphate (F1P) and pyruvate in the liver with peaks between 15–30 min post-gavage, indicative of rapid fructose absorption and hepatic fructolysis (Fig. 2d). Hepatic acetyl-CoA labeling was much slower, peaking at 60–90 min (Fig. 2d). The slower kinetic of acetyl-CoA labeling was closely aligned with the appearance of labeled acetate in the portal circulation (Fig. 2d). Labeling of hepatic fatty acids followed that of acetyl-CoA, peaking at 120–180 min (Fig. 2d), consistent with fructose feeding hepatic acetyl-CoA and fatty acid production indirectly via acetate.

We next sought to determine the source of fructose-derived acetate. While fructose is mainly taken up by the small intestine, unabsorbed fructose reaches the colon where the microbiome converts fructose into short chain fatty acids (SCFAs), including acetate[9]. To test if the microbiome is important for hepatic DNL, we depleted it with an antibiotic cocktail (Extended Data Fig. 6a–d). Antibiotic treatment slightly enhanced the appearance of labeled fructose and fructose-derived glucose in the portal vein following an oral administration of ^{13}C-fructose (Extended Data Fig. 6e–f). The induction of hepatic DNL genes following fructose consumption is thought to be dependent on fructolytic and/or glycolytic intermediates[12,23]. Consistent with normal passage of fructose from the intestine to the liver, DNL gene expression remained intact after antibiotic treatment (Extended Data Fig. 6g), as did labeling of F1P, pyruvate and citrate in the liver (Fig. 3a, Extended Data Fig. 7a). In contrast, microbiome depletion dramatically reduced the labeling from ^{13}C-fructose of hepatic acetyl-CoA and palmitate, as well as fatty acids within circulating lipids (Fig. 3a–b, Extended Data Fig. 7a–b). This reduction was well matched with depleted portal and cecal labeling of acetate and other short-chain fatty acids (Fig. 3a, Extended Data Fig. 7a, 8a–b). Antibiotic treatment also reduced total hepatic triglycerides (Extended Data Fig. 8c), consistent with prior observations[24,25]. Thus, depletion of the microbiome suppresses hepatic DNL from ^{13}C-fructose, without impairing small intestinal or hepatic fructose metabolism, or the induction of DNL gene expression.

We next investigated if acetate is a key microbial product supporting DNL. To assess whether fructose intake led to an appreciable increase in portal acetate concentrations, we measured acetate in portal and systemic blood after gavage. Portal vein acetate concentrations increased approximately twofold over baseline (to > 1 mM) at 60–90 minutes after fructose gavage (Extended Data Fig. 8d), corresponding with acetate labeling from fructose (Fig. 2d). The rise in portal acetate was absent in antibiotic treated animals (Extended Data Fig. 8d). Acetate concentrations in systemic circulation were lower than that in the portal vein and did not markedly fluctuate after fructose consumption, suggesting clearance by the liver (Extended Data Fig. 8d). Next, to assess whether acetate supports DNL downstream of microbial metabolism, mice were gavaged with ^{13}C-acetate, along with 1:1 fructose:glucose. DNL from ^{13}C-acetate, in contrast to that from ^{13}C-fructose, was not impacted by antibiotic treatment (Fig. 3c). Finally, to test if hepatic ACSS2 is required for fructose to feed DNL, ACSS2 in the liver was silenced using an adeno-associated viral hairpin targeting *Acss2*[26] (Extended Data Fig. 8e–g). Depletion of hepatic ACSS2 strongly suppressed the labeling of fatty acids in circulating lipids from ^{13}C-fructose (Fig. 3d). Altogether, these data point to a two-pronged mechanism of DNL upon consumption of a fructose bolus, in which sugar metabolism in hepatocytes triggers the DNL transcriptional program, but microbiome-dependent acetate production serves as the major fructose-derived

lipogenic substrate, after conversion to acetyl-CoA by hepatic ACSS2 (Extended Data Fig. 10a).

Distinct lipogenic signal and substrates

Microbiome-dependent acetate production from fructose occurs when rate of ingestion exceeds small intestinal uptake capacity[9]. Thus, if fructose is consumed gradually, its contribution to DNL might occur to a greater extent via ACLY, and to a lesser extent via microbial acetate production. Still, upon providing Fruc:Gluc in the drinking water, DNL was comparably stimulated in the presence or absence of ACLY (Fig. 1b). To explore this further, mice were given ^{13}C-labeled fructose or glucose in drinking water for 24 hours (Fig. 4a). Fructose-derived carbons provided a substantial contribution to hepatic lipid pools, with greater than 20% of total liver fatty acid carbons being labeled from ^{13}C-fructose after 24 hours of Fruc:Gluc drinking, while ^{13}C-glucose contributed less (Fig. 4b). In this context, ACLY deficiency reduced ^{13}C-fructose and -glucose labeling of fatty acids (Fig. 4b). Nevertheless, total DNL as measured by D_2O labeling was not different between genotypes (Fig. 4c), indicating sufficient availability of other two-carbon donors. One possibility is assimilation of acetate from other sources (e.g. fiber fermentation). To test this, we supplemented Fruc:Gluc drinking water with ^{13}C-acetate upon initial exposure (naïve) and after 2 weeks on Fruc:Gluc water (conditioned) (Extended Data Fig. 9a). Fatty acid labeling from ^{13}C-acetate was higher in LAKO mice at baseline (Fig. 4d). After fructose conditioning, acetate contribution to DNL increased in WT animals, and this was further enhanced in LAKO mice (Fig. 4d), consistent with increased hepatic ACSS2 expression in LAKO mice following fructose feeding, which preceded the onset of steatosis (Extended Data Fig. 9b–c). We next assessed the contribution of microbiome-derived acetate from all dietary sources in the context of gradual fructose consumption. Antibiotic treatment suppressed total hepatic DNL in LAKO mice (Fig. 4e, Extended Data Fig. 9d). ChREBPβ and DNL gene expression were confirmed to be upregulated by Fruc:Gluc drinking in all groups, indicating that their regulation in response to fructose consumption is independent of acetyl-CoA metabolism (Fig. 4f). Finally, we examined DNL in Fruc:Gluc-drinking mice following silencing of hepatic ACSS2, finding that in the context of gradual fructose consumption via drinking water, loss of both ACLY and ACSS2 is necessary to suppress DNL (Fig. 4g). These data indicate that when fructose is consumed gradually to reduce its passage into the colon, the rate of DNL is established by signaling mechanisms (i.e., sugar-driven ChREBP activation), and DNL is suppressed only when acetyl-CoA production by both ACLY and ACSS2 is inhibited (Extended Data Fig. 10b).

Discussion

This study demonstrates that bolus fructose consumption triggers hepatic DNL independent of liver ACLY but dependent on fructose metabolism to acetate by gut microbiota, which reaches the liver via the portal vein. The induction of the DNL transcriptional program in the liver, however, appears to be independent of both ACLY and the microbiome, consistent with evidence that hexose-phosphate metabolites are important for ChREBP activation[19,27]. This likely explains why KHK knockout mice are protected from fructose-induced fatty liver[28,29]. Thus, we propose a revised model of fructose-dependent DNL induction, in which

hepatic fructose metabolism provides a signal to transcriptionally promote DNL while microbial fructose metabolism provides acetate to feed DNL (Extended Data Fig. 10a). These dual mechanisms may also explain higher lipogenic potential of fructose as compared to glucose[30], at least in the context of high dose sugar consumption, in that the small intestine rapidly absorbs even large loads of glucose, whereas fructose reaches the gut microbiome, which generates acetate[9]. When consumed more gradually, fructose can feed DNL in an ACLY-dependent manner. However, acetate from other sources is also readily available to the liver, rendering ACLY dispensable for DNL even when fructose is gradually consumed (Extended Data Fig. 10b). Of note, acetate is likely insufficient to trigger DNL in the absence of the sugar-derived lipogenic signal. Thus, it will be important in the future to define how fructose interacts with dietary sources of acetate such as ethanol and fermentable fibers.

Understanding the fundamental pathways involved in hepatic DNL is important for the development of new therapeutic interventions for metabolic diseases. In addition to acetate, the microbiome also produces other SCFAs such as butyrate and propionate. Butyrate has been shown to contribute to hepatic lipogenesis[31], but likely feeds extra-mitochondrial acetyl-CoA pools in an ACLY-dependent manner[32]. Diet and microbiome could potentially impact the efficacy of ACLY inhibitors, currently in clinical trials for hypercholesterolemia[33]. Prior studies of RNAi-mediated ACLY deficiency report decreased hepatic lipid in *db/db* mice and mice fed a high-fat, high sucrose diet, but increased hepatic lipid in mice fed a high fat diet only[34,35,36]. In our own data, principal component analysis of hepatic triglycerides separated LAKO mice from WT mice on HFrD but not on chow (Extended Data Fig. 3c), supportive of the notion that ACLY may play distinct roles depending on diet. The current data elucidate a previously unappreciated interplay between diet, the gut microbiome, and host organ metabolism that contributes to fructose-induced NAFLD.

Methods

Generation of Liver-specific ACLY Knockout (LAKO) mice

Generation of $Acly^{f/f}$ mice on a C57Bl6/J background was previously described[10]. To generate hepatocyte-specific *Acly* knockouts, $Acly^{f/f}$ mice were crossed to albumin-Cre transgenic mice (B6.Cg-Tg(Alb-Cre)21Mgn/J, Jackson Laboratory)[37].

Genotying

Genotyping of the recombined Acly allele was confirmed as previously described[10]. Genotyping of the Albumin-Cre allele was confirmed with the following primer sequences: AlbCre-5'F (CCTGCCAGCATGGATATAA), AlbCre-3'R (GTTGTCCTTTGTGCTGCTGA), Alb-TSP3 (GAAGCAGAAGCTTAGGAAGATGG), and the following cycling conditions: 1 cycle - 94° × 5 min. 35 cycles - 94° × 45 sec., 58° × 45 sec., 72° × 1 min. 1 cycle - 72° × 10 min, hold at 4°C.

Animal studies

All animal protocols in this study were approved by the University of Pennsylvania's Institutional Animal Care and Use Committee (IACUC) and Princeton University's IACUC. For diet studies, 4-week-old male mice were placed on either a regular chow diet (Lab Diet 5010) or a high-fructose chow diet (Teklad TD.89247) for indicated lengths of time. Weights of mice kept on each diet were taken weekly. For drinking water studies, mice were provided with regular tap water (filtered through a 0.22 μm filter) or a 15% (w/v) fructose:15% (w/v) glucose (Sigma F3510, G8270) in tap water (filtered through a 0.22 μm filter). To deplete the gut microbiome, mice were given a daily 10 μL/g body weight oral gavage consisting of 1 mg/mL ampicillin, 1 mg/mL gentamicin, 0.5 mg/mL vancomycin, 1 mg/mL neomycin, 1 mg/ml metronidazole in a 0.9% NaCl solution for 7–10 days. Studies were controlled to mice given the same 0.9% NaCl solution without antibiotics. To knockdown *Acss2*, 6–8 week-old male mice were injected via tail vein with 2.0×10^{11} GC/mouse AAV8.U6.shAcss2.CMV.eGFP.SV40 (University of Pennsylvania Vector Core) or AAV8.CMV.PI.eGFP.WPRE.bGH (Addgene) as control; experiments were performed 1 week after injection.

Histology

For H&E, Periodic Acid Shiff, Trichrome staining: tissues were fixed in formalin overnight, dehydrated by titrating in ethanol (50%, 75%, 95%), and submitted to the Molecular Pathology and Imaging Core at the University of Pennsylvania for paraffin embedding, sectioning, and staining. For Oil Red O staining: tissues were fixed in formalin overnight, dehydrated by titrating in sucrose (10%, 20%, 30%), and embedded in Richard-Allan Scientific NEG-50 frozen section medium (ThermoFisher Scientific 6502) by freezing in 2-methylbutane that was cooled using dry ice. Tissues frozen in NEG-50 were submitted to the Molecular Pathology and Imaging Core at the University of Pennsylvania for cryosectioning and staining. Images were acquired on a Keyence BZ-X710 microscope.

Bacterial quantification

Cecal contents were collected, snap frozen, and weighed before storage in −80C until use. DNA was extracted from cecal contents using a Fecal DNA extraction kit (IBI scientific IB47821) according to manufacturer instructions. Samples were diluted 1:1000 prior to use for RT-PCR. To establish a bacterial DNA standard, genomic DNA was extracted from *Stbl3* E. coli cells. A standard curve was generated using a 1:4 serial dilution starting with 10 ng of E. coli DNA. RT-PCR was performed as described, using previously published universal 16s primers (Forward: TCCTACGGGAGGCAGCAGT, Reverse: GGACTACCAGGGTATCTAATCCTGTT)[38]. Relative bacterial load was calculated by normalizing DNA content to initial cecal content weight.

Immunoblotting

Protein extraction from tissue was performed by re-suspending frozen tissue in 0.5 mL of RIPA buffer (1% NP-40, 0.5% Deoxycholate, 0.1% SDS, 150 mM NaCl, 50 mM Tris plus protease and phosphatase inhibitors), and lysed using a tissue lyser (Qiagen) twice for 30 seconds at 20 Hz. Following lysis, samples were incubated on ice for 10 minutes, then spun

down at 15,000 RCF for 5 minutes in 4°C. Supernatant was collected and stored in −80°C until immunoblotting. Antibodies used in this study: ATP-Citrate Lyase (Proteintech 15421–1-AP), Acyl-CoA Synthetase Family Member 2 (Cell Signaling Technology 3658S), Acetyl-CoA Carboxylase (Cell Signaling Technology 3676S), Fatty Acid Synthase (Cell Signaling Technology 3189S), Catalase (Cell Signaling Technology 14097S), Ribosomal Protein S6 (Cell Signaling Technology 2217S), IRDye800CW Goat Anti-Rabbit (LI-COR 926–32211). Immunoblots were developed using a LI-COR Odyssey Clx.

Quantitative RT-PCR

RNA extraction from tissue was performed by re-suspending frozen tissue in 1 mL Trizol (Life Technologies), and lysed using a tissue lyser (Qiagen) for 60 seconds at 30 Hz, followed by manufacturer protocol for Trizol RNA extraction. cDNA was synthesized using high-capacity RNA-to-cDNA master mix (Applied Biosystems 4368814), as per the kit instructions. cDNA was diluted 1:20 and amplified using PowerUp SYBR Green Master Mix (Applied Biosystems A25778) on the ViiA-7 Real-Time PCR system. Fold change in expression was calculated using ΔCt, with 18S reference gene as an endogenous control. Primer sequences for RT-qPCR are: Aldob (Forward: GAAACCGCCTGCAAAGGATAA, Reverse: GAGGGTCTCGTGGAAAAGGAT), Khk (Forward: ATGTGGTGGACAAATACCCAGA, Reverse: CAAGCAAGGAAAGGACAGTGC), Acly (Forward: TTCGTCAAACAGCACTTCC, Reverse: ATTTGGCTTCTTGGAGGTG), Acss2 (Forward: GCTTCTTTCCCATTCTTCGGT, Reverse: CCCGGACTCATTCAGGATTG), Chrebpα (Forward: CGACACTCACCCACCTCTTC, Reverse: TTGTTCAGCCGGATCTTGTC), Chrebpβ (Forward: TCTGCAGATCGCGTGGAG, Reverse: CTTGTCCCGGCATAGCAAC), Fasn (Forward: ATTGGTGGTGTGGACATGGTC, Reverse: CCCAGCCTTCCATCTCCTG), Acc1 (Forward: ACAGTGGAGCTAGAATTGGAC, Reverse: ACTTCCCGACCAAGGACTTTG).

Measurement of *de novo* lipogenesis using isotope tracers

To assess total lipogenesis, mice were provided with 50% (v/v) deuterated water (Sigma 151882) mixed into 15% fructose:15% glucose drinking water for 24 hours. Systemic blood was collected by cardiac puncture, allowed to coagulate on ice for 10 minutes, and spun down at 15,000 × RCF for 10 minutes at 4°C to collect serum. To account for differences in drinking water consumption, calculated deuterium enrichment labeling in serum water was used to normalize labeling into fatty acids. To assess lipogenesis from dietary carbohydrates, on day of experiment, mice were weighed and fasted from 10 a.m. until 3 p.m., when they were given an oral gavage consisting of a 1:1 mixture of glucose and fructose in a 0.9% NaCl saline. Doses used in this study ranged from 1.0 g/kg or 2.0 g/kg of each hexose. [U-^{13}C]-glucose (CLM-1396–1) or [U-^{13}C]-fructose (CLM-1553–1) were provided with the corresponding unlabeled hexose. Six hours following gavage, systemic blood was collected by tail bleeding the mice and incubating the blood on ice for 15 minutes before spinning down at 15,000 × RCF for 10 minutes at 4°C to collect serum. Tissues were collected using a clamp pre-cooled with liquid nitrogen. The frozen liver samples were ground at liquid nitrogen temperature with a Cryomill (Retsch, Newtown, PA). Saponification of lipids and LC-MS analysis were performed as previously described[39]. Briefly, serum (5 μL) or liver

powder (10 mg) was incubated with 1 mL of 0.3 M KOH in 90% methanol at 80°C for 1 hour in a 2 mL glass vial. Formic acid (0.1 mL) was then added for neutralization. The saponified fatty acids were extracted by adding 0.5 mL of hexane, vortexing, and transferring the top hexane layer to a new glass vial. Samples were then dried under a stream of N2 and dissolved in 100 μL (for serum) or 1 mL (for liver) of isopropanol:methanol (1:1, v/v) solution for LC-MS analysis. Separation was performed by reversed-phase ion-pairing chromatography on a C8 column coupled to negative-ion mode, full-scan LC-MS at 1-Hz scan time and 100,000 resolving power (stand-alone orbitrap; Thermo Fischer Scientific). Data analysis with MAVEN software and natural isotope correction were performed as previously described[40].

Primary Hepatocyte Isolation

Hepatocytes were isolated using a two-step collagenase/DNAse digestion protocol[41] and plated in M199 media containing 5 mM glucose, 10% FBS, 500 nM dexamethasone and 1 nM insulin. Following attachment, cells were changed to M199 media containing 5 mM glucose, 500 nM dexamethasone and incubated overnight. Cells were switched to M199 containing 5 mM glucose, 10% FBS, 500 nM dexamethasone, 100 nM insulin and respective fructose and acetate supplementation for 6 hours on day of experiment. Evidence that high concentrations of glucose are required to induce the DNL gene program in primary hepatocytes[42] informed our use of 25 mM fructose.

Acyl-CoA measurements in primary hepatocytes

Acyl-CoA measurements in primary hepatocytes were performed by liquid chromatograpy-mass spectrometry/high-resolution mass spectrometry (LC-MS/HRMS) as previously described[43]. Briefly, primary hepatocytes were isolated and cultured as described above in 6-well plates. At harvest, culture media was completely aspirated before harvesting cells in 0.5 mL ice-cold 10% trichloroacetic acid/well of a 6-well dish using a cell lifter. Samples were then sonicated for 10 × 0.5 second pulses to completely disrupt cellular membranes, and incubated on ice to precipitate proteins. Protein was pelleted at 16,000 × RCF for 10 minutes at 4°C. Supernatant was collected and purified by solid-phase extraction using Oasis HLB 1cc (30 mg) SPE columns (Waters). Eluate was evaporated to dryness under nitrogen gas and re-suspended in 50 μL of 5% 5-sulfosalicylic acid (w/v) for injection. Samples were analyzed by an Ultimate 3000 autosampler coupled to a Thermo Q-Exactive Plus instrument in positive electrospray ionization (ESI) mode. For isotopic tracer analysis, isotopic enrichment from [U-^{13}C]-fructose (Cambridge Isotope Laboratories, CLM-1553) or [U-^{13}C]-acetate (Cambridge Isotope Laboratories, CLM-440–1) was calculated to compensate for the non-linearity of isotopic enrichment using the FluxFix calculator[44].

Fructolyic measurements in primary hepatocytes

For fructolytic intermediate measurements in primary hepatocytes, culture media was completely aspirated before harvesting cells in 0.5 mL of cold 80:20 methanol:water/well of a 6-well dish using a cell lifter. Samples were then sonicated for 10 × 0.5 second pulses to completel disrupt cellular membranes, and incubated on ice. Samples were then spun down at 16,000 × RCF for 10 minutes at 4°C. Supernatant was collected and dried under nitrogen gas flow in preparation for water-soluble metabolomic analysis.

Chromatin Immunoprecipitation (ChIP) – PCR

For H3K27ac-ChIP qPCR studies, WT male mice were provided with Fruc:Gluc drinking water for 24 hours, and orally gavaged with 2.0 g/kg fructose + 2.0 g/kg glucose 1 hour prior to sacrifice. ChIP was performed as previously described[45] with adjustments to start from liver tissue. Liver tissues were harvested from mice 90 minutes following gavage, and 100 mg of tissue was weighed out. Tissues were homogenized by mincing briefly with razor blades followed by resuspension in 5 mL of ice-cold 1X PBS and several passages through a 16 gauge syringe needle into 15 mL conical tubes. Samples were crosslinked with 2% formaldehyde for 10 minutes at room temperature. The reactions were quenched with 0.25 M glycine. The cells were then washed with 1X PBS and resuspended in cell lysis buffer (10 mM Tris-HCl pH 8.1, 10 mM NaCl, 1.5 mM $MgCl_2$, 0.5% NP-40), supplemented with protease inhibitors (Roche). The cell pellet was resuspended in 0.5 mL of nuclear lysis buffer (50 mM Tris-HCl pH 8.1, 5 mM EDTA, 1% SDS) supplemented with protease inhibitors. The chromatin was fragmented with a Diagenode Bioruptor Pico (12 cycles of 30 s on followed by 30 s off, at 4°C). Samples were incubated with protein G magnetic beads (Millipore-Sigma 16–662) and H3K27ac (Abcam ab4729), ChREBP (Novus Biologicals NB400–135), or Normal Rabbit IgG (Cell Signalling Technology 2729S) antibody overnight at 4°C. The next day, samples were washed 5 times with decreasingly stringent buffers. ChIP DNA was eluted off the beads by incubating beads in 125 μL elution buffer for 10 minutes at 65°C. The combined supernatant was then incubated overnight at 65°C to reverse crosslinks and proteinase K treated for 1 hour the next morning. Samples were purified using Macherey-Nagel DNA purification kit, with NTB binding buffer. Samples were diluted 1:5 in nuclease-free water prior to RT-qPCR reactions, which were performed as described above with the following primers: Mlxipl p1 (Forward: CGCACCCGGTCTACAGTTT, Reverse: GTGCCTCCTTCTCTCCTTAGC), Mlxipl p2 (Forward: GCCATCCACGTGCTAAGGA, Reverse: GGCTTTTAGACTGGGGTGTGG), Pklr p1 (Forward: GGGAAGGATGCCCACTACAG, Reverse: TGGAAGCCTTGTACACTGGG), Pklr p2 (Forward: CCCAGTGTACAAGGCTTCCAT, Reverse: CTCTGCCTTTGTCAGTGGGA), Acss2 p1 (Forward: ATTGGATGCCTAGAGCACGG, Reverse: CGCATCAAGTTCCGAACACC), Acss2 p2 (Forward: TCAGGACAGTTTAGGGTGCAA, Reverse: TTACAAAGACCTGCCTCTGCC).

Triglyceride Measurements

Triglyceride measurements were performed using a Triglyceride Colorimetric Assay Kit (Cayman Chemical 10010303) as per manufacturer instructions.

Metabolomics

Water-soluble metabolite extraction was performed as previously described[9]. For serum samples, 100 μL −20°C methanol was added to 5 μL of serum sample and incubated on ice for 10 min, followed by vortexing and centrifugation at 16,000 × g for 10 min at 4°C. The supernatant (first extract) was transferred to a new tube. Then, 50 μL methanol was added to resuspend the pellet, followed by vortexing and centrifugation at 16,000 × g for 10 min at 4°C. The supernatant (second extract) was combined with the first extract. Then, 3 μL of the 150 μL extract was loaded to LC-MS. For tissue samples, frozen tissue samples were ground

at liquid nitrogen temperature with a Cryomill (Retsch, Newtown, PA). The resulting tissue powder was weighed (~20 mg). The extraction was then done by adding −20°C 40:40:20 methanol:acetonitrile:water to the powder and incubating in −20°C overnight, followed by vortexing and centrifugation at 16,000 × g for 10 min at 4°C. The volume of the extraction solution (μL) was 40 × the weight of tissue (mg) to make an extract of 25 mg tissue per mL solvent. Serum and tissue extracts were analyzed by LC-MS, using two different LC-MS methods chosen for optimal separation of glucose and fructose (in serum) and of hexose phosphate species (from tissues). Serum extracts were analyzed (without drying) using a quadrupole-orbitrap mass spectrometer (Q Exactive, Thermo Fisher Scientific, San Jose, CA) operating in negative ion mode, coupled to hydrophilic interaction chromatography via electrospray ionization and used to scan from m/z 70 to 1000 at 1 Hz and 75,000 resolution. LC separation was on a XBridge BEH Amide column (2.1 mm × 150 mm, 2.5 μm particle size, 130 Å pore size) using a gradient of solvent A (20 mM ammonium acetate, 20 mM ammonium hydroxide in 95:5 water: acetonitrile, pH 9.45) and solvent B (acetonitrile). Flow rate was 150 μl/min. The LC gradient was: 0 min, 85% B; 2 min, 85% B; 3 min, 80% B; 5 min, 80% B; 6 min, 75% B; 7 min, 75% B; 8 min, 70% B; 9 min, 70% B; 10 min, 50% B; 12 min, 50% B; 13 min, 25% B; 16 min, 25% B; 18 min, 0% B; 23 min, 0% B; 24 min, 85% B; 30 min, 85% B. Autosampler temperature was 5°C, and injection volume was 3 μL. Tissue extracts were dried under nitrogen gas flow and re-dissolved in LC-MS grade water. Metabolites were analyzed via reverse-phase ion-pairing chromatography coupled to an Exactive Orbitrap mass spectrometer (Thermo Fisher Scientific, San Jose, CA). The mass spectrometer was operated in negative ion mode with resolving power of 100,000 at m/z 200 and scan range of m/z 75–1000. The LC method was modified from an earlier method (Lu et al., 2010), using an Atlantis T3 column (150 mm × 2.1 mm, 3 μm particle size, 100 Å pore size), with a gradient of solvent A (97:3 water:methanol with 10 mM tributylamine and 15 mM acetic acid) and solvent B (methanol). The LC gradient was 0 min, 0% B, 200 μl/min; 2 min, 0% B, 200 μl/min; 4 min, 20% B, 200 μl/min; 13 min, 80% B, 200 μl/min; 17 min, 100% B, 200 μl/min; 17.5 min, 100% B, 300 μl/min; 20 min, 100% B, 300 μl/min; 20.5 min, 0% B, 300 μl/min; 24 min, 0% B, 300 μl/min; 25 min, 0% B, 200 μl/min. Other LC parameters, common to both methods, were column temperature 25°C, autosampler temperature 5°C, and injection volume 10 μL. Data analysis with MAVEN software and natural isotope correction were performed as previously described[40]. Volcano plot and principle component analysis of metabolomics data were generated using Metaboanalyst[46].

Acetate measurement

Acetate was derivatized and measured by LC-MS. The derivatizing reagent was 12 mM EDC, 15 mM 3-Nitrophenylhydrazine and pyridine (2% v/v) in methanol. Reaction was stopped with quenching reagent consisting of 0.5 mM beta-mercaptoethanol in water. Serum (5 μL) was mixed with derivatizing reagent (100 μL) and incubated for 1 hour at 4°C. Then, the samples were centrifuged at 16,000 × g for 10 min at 4°C, and 20 μL of supernatant was mixed with 200 μL of the quenching reagent. After centrifugation at 16,000 × g for 10 min at 4°C, supernatants were collected for LC-MS analysis. A quadrupole-time of flight mass spectrometer (Q-TOF, Agilent, Santa Clara, CA) operating in negative ion mode was coupled to C18 chromatography via electrospray ionization and used to scan from m/z 100 to 300 at 1 Hz and 15,000 resolution. LC separation was on an Acquity UPLC BEH C18

column (2.1 mm × 100 mm, 1.7 5 μm particle size, 130 Å pore size; Waters, Milford, MA) using a gradient of solvent A (0.01% formic acid in water) and solvent B (0.01% formic acid in isopropanol). Flow rate was 400 μL/min, except that from 6 min to 8 min flow rate was increased to 700 μL/min. The LC gradient was: 0 min, 10% B; 2 min, 15% B; 5 min, 25% B; 6 min, 100% B; 8 min, 100% B; 8.6 min, 10% B; 10.5 min, 10% B. Autosampler temperature was 5°C, and injection volume was 10 μL. Ion masses for derivatized acetate was 194.

Lipidomics

Lipidomics was performed as previously described[47], with some modifications on an extraction step. Briefly, serum samples (10 μL) was dissolved in 100 μL of isopropanol. After centrifugation at 14,000 g at 4°C for 10 min, supernatant was transferred to a glass MS vial and injected into a 1290 Infinity UHPLC system coupled to Agilent 6550 iFunnel Q-TOF mass spectrometer. To cover both the positive charged and negative charged species, each sample was analyzed twice using the same LC gradient but with different mass spectrometer ionization modes. The LC separation was performed on an Agilent Poroshell 120 EC-C18 column (150 × 2.1 mm, 2.7 μm particle size) with a flow rate of 150 μL/min. Solvent A was 1 mM ammonium acetate + 0.2% acetic acid in water/methanol (90:10). Solvent B was 1 mM ammonium acetate + 0.2% acetic acid in methanol/2-propanol (2:98). The solvent gradient in volume ratios was as follows: 0–2 min, 25% B; 2–4 min, 25 to 65% B; 4–16 min, 65 to 100% B; 16–20 min, 100% B; 20–21 min, 100 to 25% B; 21–27 min, 25% B. Principle component analysis was generated using Metaboanalyst[46] (https://www.metaboanalyst.ca) and heatmap of lipidomics data was generated using Morpheus (https://software.broadinstitute.org/morpheus).

Extended Data

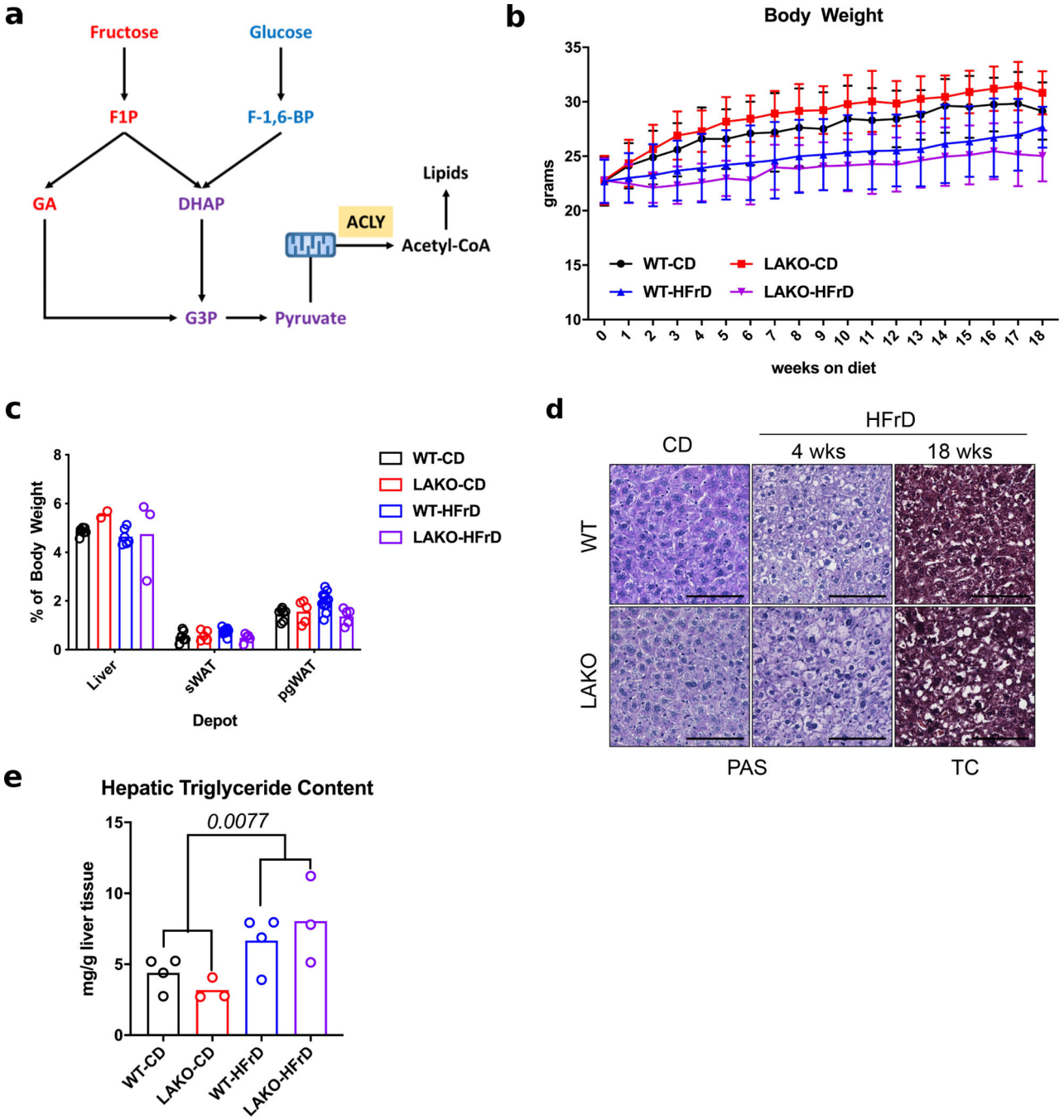

ED Figure 1. Hepatic ACLY deficiency minimally impacts the response to dietary fructose.

a, Schematic of fructolysis and glycolysis feeding into de novo lipogenesis. F1P = fructose-1-phosphate, F-1,6-BP = fructose-1,6-bisphosphate, GA = glyceraldehyde, DHAP = dihydroxyacetone phosphate, G3P = glyceraldehyde-3-phosphate. **b**, Body weights of WT and LAKO mice on CD or HFrD for 18 weeks (n = WT-CD:13, LAKO-CD:5, WT-HFrD:14, LAKO-HFrD:5), data are mean ± SD. **c**, Weights of liver, posterior subcutaneous (sWAT) and perigonadal (pgWAT) adipose tissues in WT and LAKO mice on CD or HFrD for 18 weeks (n Liver/sWAT/pgWAT = WT – CD: 7/7/7, LAKO – CD: 2/5/5, WT – HFrD: 6/12/12,

LAKO – HFrD: 3/5/5). **d**, Representative images of Periodic Acid Schiff (PAS) stain for glycogen and Trichrome (TC) histological stain for fibrosis in livers from WT or LAKO mice on HFrD. Scale bars = 100 μm. **e**, Triglyceride content in WT or LAKO mice on CD or HFrD for 18 weeks, n = (WT-CD: 4, LAKO-CD: 3, WT-HFrD: 4, LAKO-HFrD: 3), statistical significance determined using Welch's t test. For panels c and e, bars represent mean.

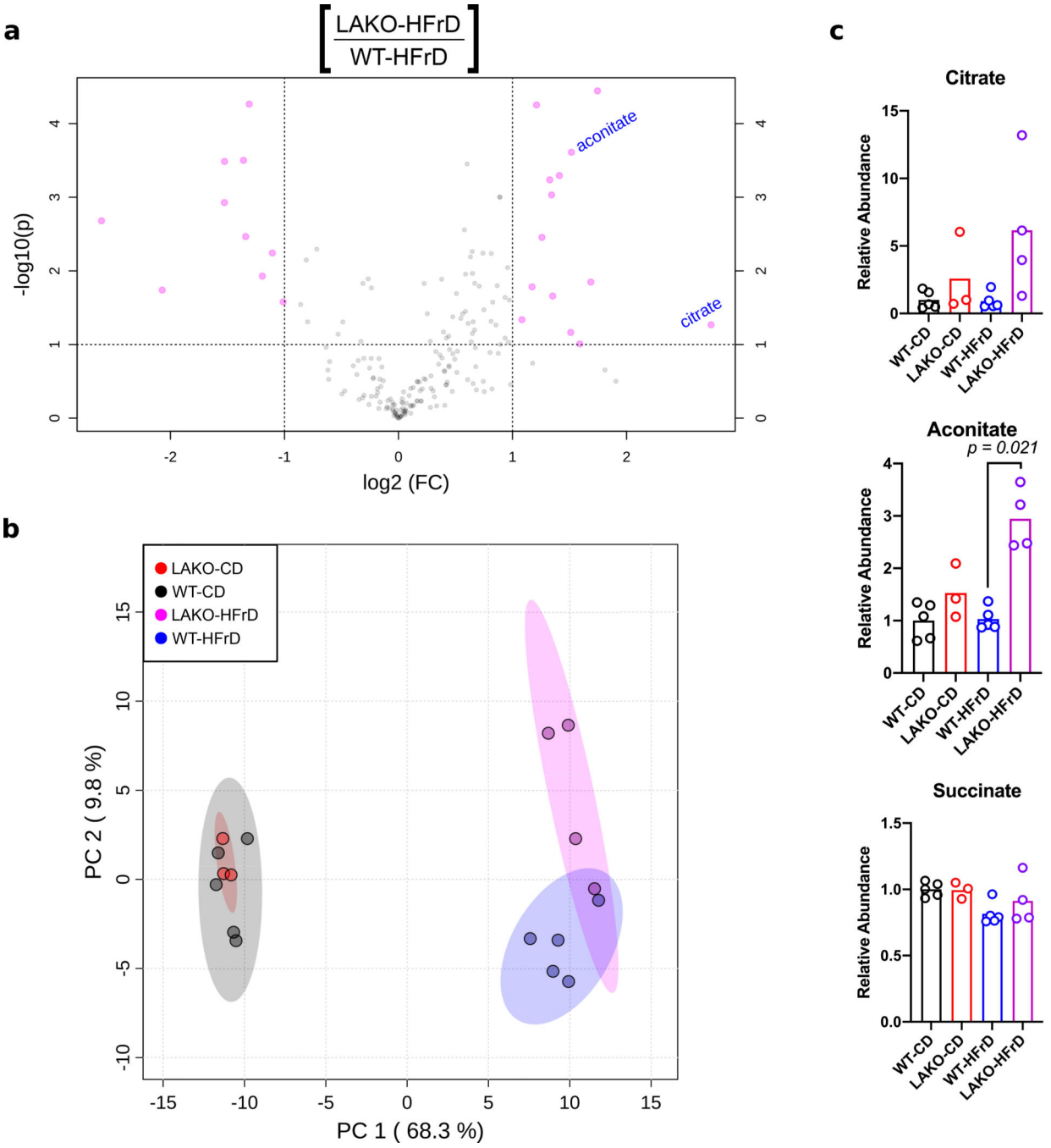

Extended Data Figure 2. Hepatic ACLY deficiency results in modest metabolic alterations on high fructose diet.

a, Volcano plot of hepatic metabolites in WT and LAKO mice on CD or HFrD for 4 weeks, pink dots indicate significant hits as determined by a fold-change threshold of 2 and P-value threshold of 0.1, assuming equal variance. **b**, Principle component analysis of log-transformed data in Supplementary Table 1, each dot represents a unique sample, 95% CI shown in corresponding color. **c**, Relative metabolite abundance, normalized to WT-CD

group, *p* values determined using Welch's t test, n = (WT-CD:5, LAKO-CD: 3, WT-HFrD: 5, LAKO-HFrD: 4). Bars represent mean.

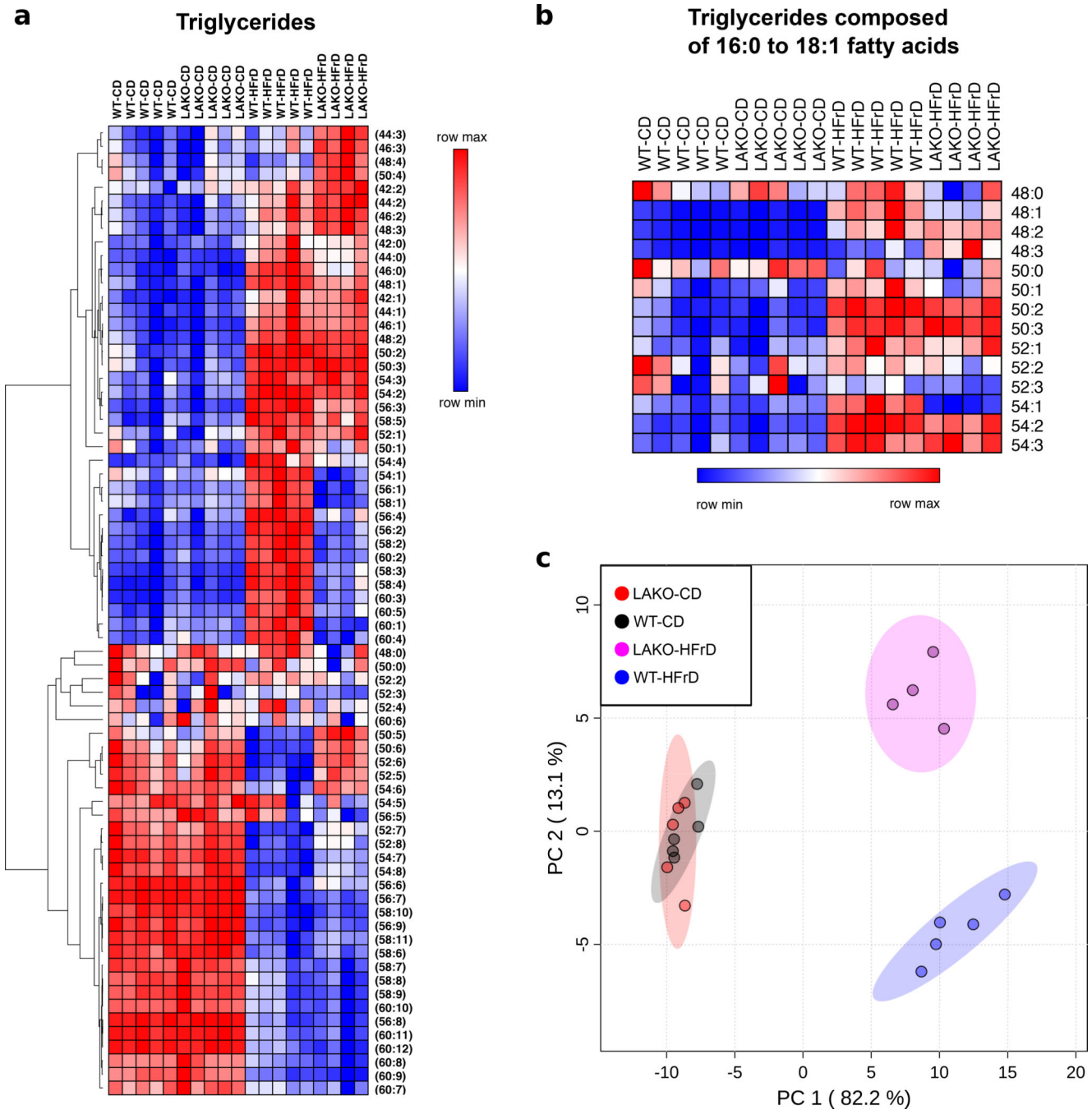

Extended Data Figure 3. High fructose diet alters hepatic lipid metabolism.

a, Hierarchical clustering of relative hepatic triglyceride abundance in WT or LAKO mice on CD or HFrD for 4 weeks, clustering performed using one minus pearson correlation and average linkage. **b**, Relative abundance of hepatic triglycerides composed of 16:0 to 18:1 fatty acids, subset of data in panel **a**. **c**, Principle component analysis of log-transformed data in Supplementary Table 2, each dot represents a unique sample, 95% CI shown in corresponding color.

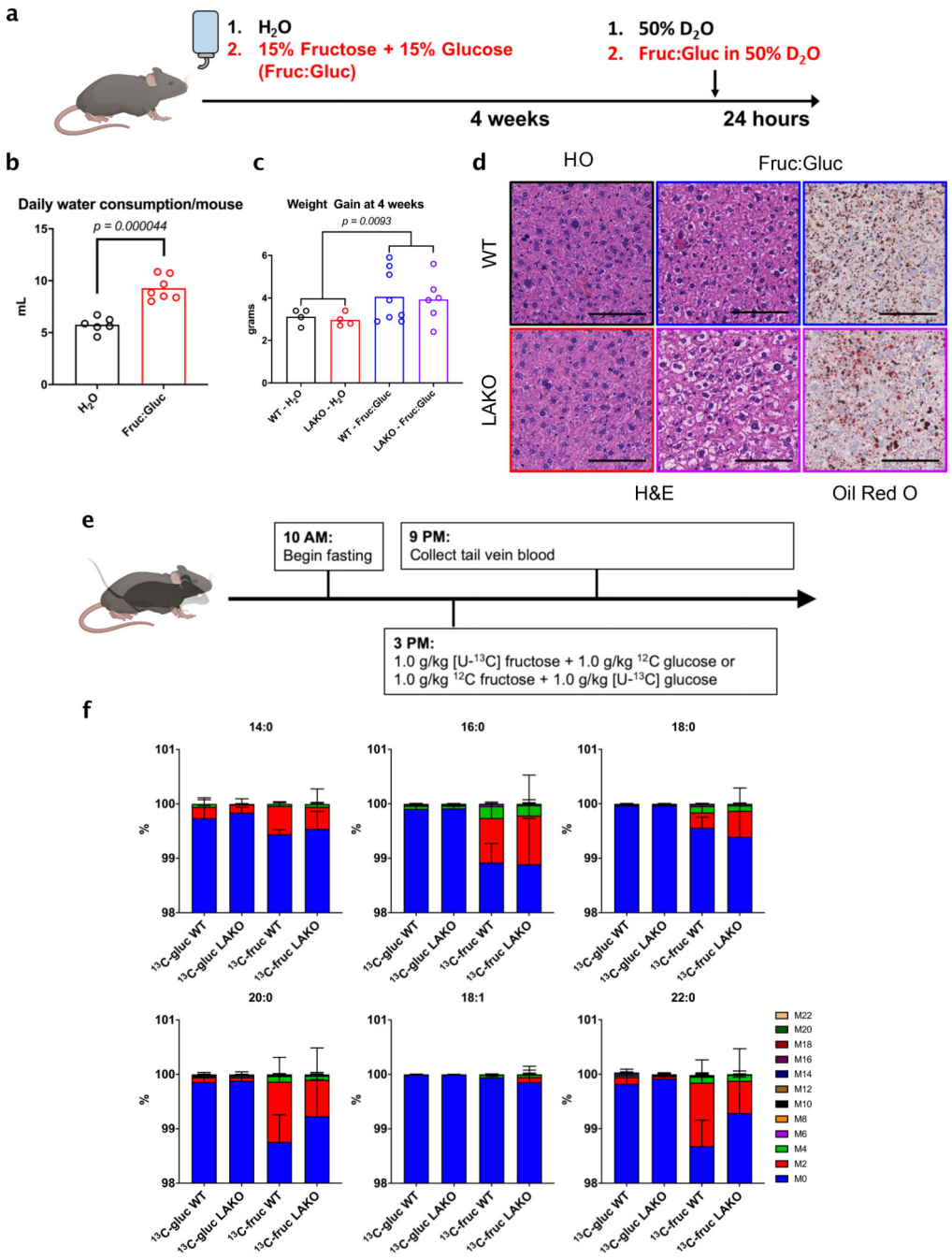

Extended Data Figure 4. Fructose induces steatosis and contributes substantially to newly synthesized fatty acids in the liver independently of ACLY.

a, Schematic of experimental design of drinking water study. **b**, Daily consumption of unsweetened (H_2O) or 15% fructose + 15% glucose sweetened (Fruc:Gluc) water per mouse, each dot represents a repeat measurement (n = H_2O: 6, Fruc:Gluc: 7), statistical significance determined using Welch's t test. **c**, Weight gain of WT or LAKO mice given H_2O or Fruc:Gluc water for 4 weeks (n = WT – H_2O: 4, LAKO – H_2O: 4, WT – Fruc:Gluc: 8, LAKO Fruc:Gluc: 6), *p* value indicated comparing all H_2O vs. Fruc:Gluc mice determined by Welch's t test. **d**, Representative H&E and Oil Red O histological stains of

livers from mice in panel **c**. Scale bars = 100 μm. **e**, Experimental design for data shown in Figure 1c. **f**, Isotopologue distribution of labeled serum saponified fatty acids shown in Figure 1c. For all panels, data are mean ± SD.

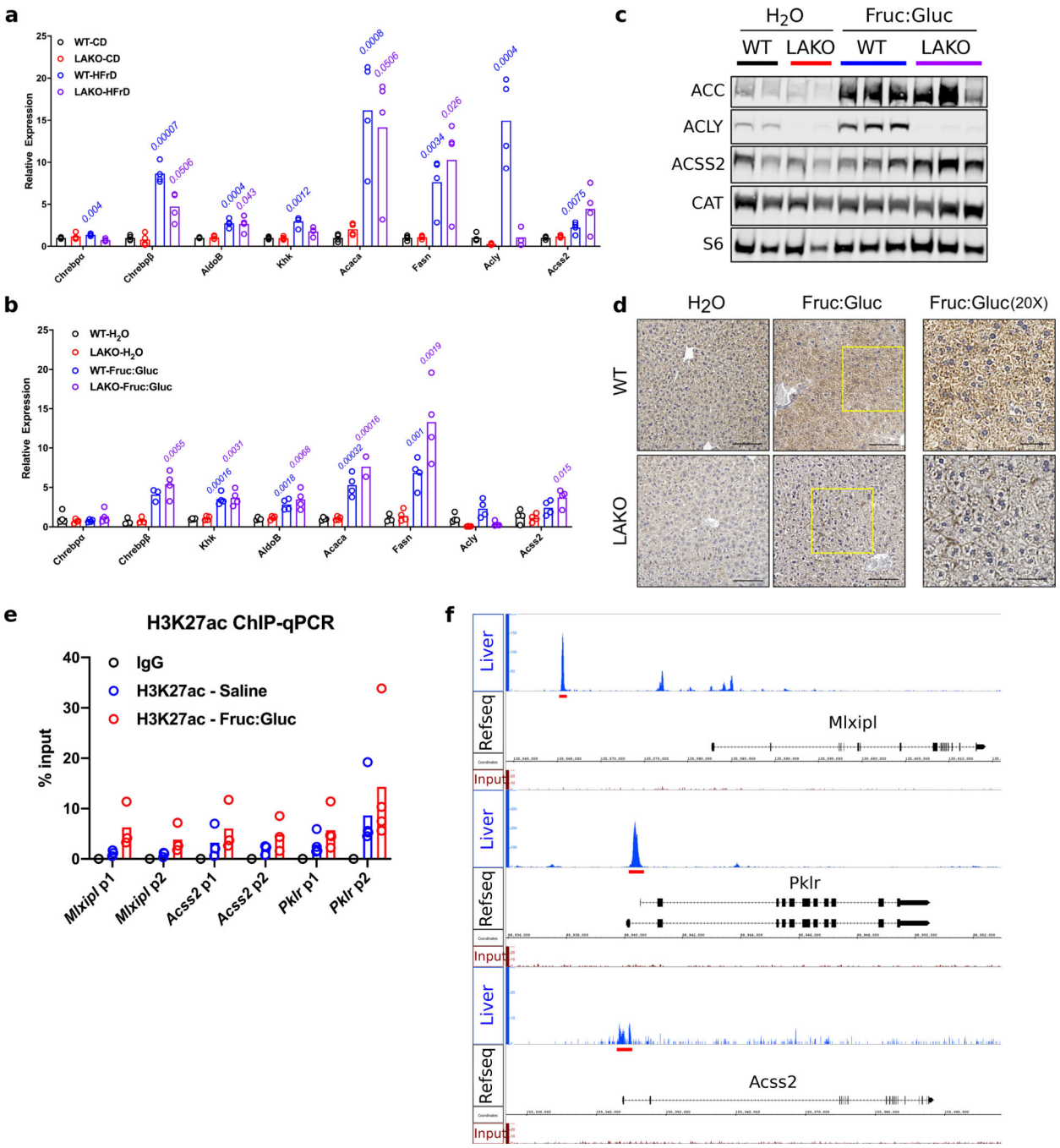

Extended Figure Data 5. Fructose signals the use of acetate for de novo lipogenesis.

a, mRNA expression of ChREBP and its target genes in livers of WT or LAKO mice fed CD or HFrD (n = 4 mice/group), *p* values for WT-CD vs. WT-HFrD (blue text) and LAKO-CD vs. LAKO-HFrD (purple text) determined using two-sided t tests with Holm-Sidak method for multiple comparisons. **b**, mRNA expression of lipogenic genes in livers of WT or LAKO mice given H_2O or Fruc:Gluc water for 4 weeks (n = 4/group), statistical comparisons WT-H_2O vs. WT-Fruc:Gluc, *p* values for WT – H_2O vs. WT – Fruc:Gluc (blue font) and LAKO – H_2O vs. LAKO Fruc:Gluc (purple font) determined using two-sided t test with Holm-

Sidak method for multiple comparisons. **c**, Immunoblots of lipogenic enzymes in livers of WT or LAKO mice given H_2O or Fruc:Gluc water for 4 weeks, each lane represents an individual mouse. **d**, Immunohistochemistry staining against ACLY in WT or LAKO livers on H_2O or Fruc:Gluc water for 4 weeks. Yellow boxes approximate location of 20X panels. Scale bars = 100 μm for 10X, 50 μm for 20X. **e**, H3K27ac ChIP-qPCR of livers from WT mice provided either water for 24 hours followed by an oral gavage of saline, or Fruc:Gluc water for 24 hours, followed by an oral gavage of 2.0 g/kg glucose and 2.0 g/kg fructose (Mlxipl: n = 3, Acss2: n = 3, Pklr: n = 4), livers harvested 90 minutes after gavage. p1 and p2 are two different primer sets. **f**, ChIP-seq tracks of Mlxipl, Pklr, Acss2 genomic loci[16], red bars indicate genomic regions used to design ChIP-qPCR primers. For panels a-b and e-f, bars represent mean.

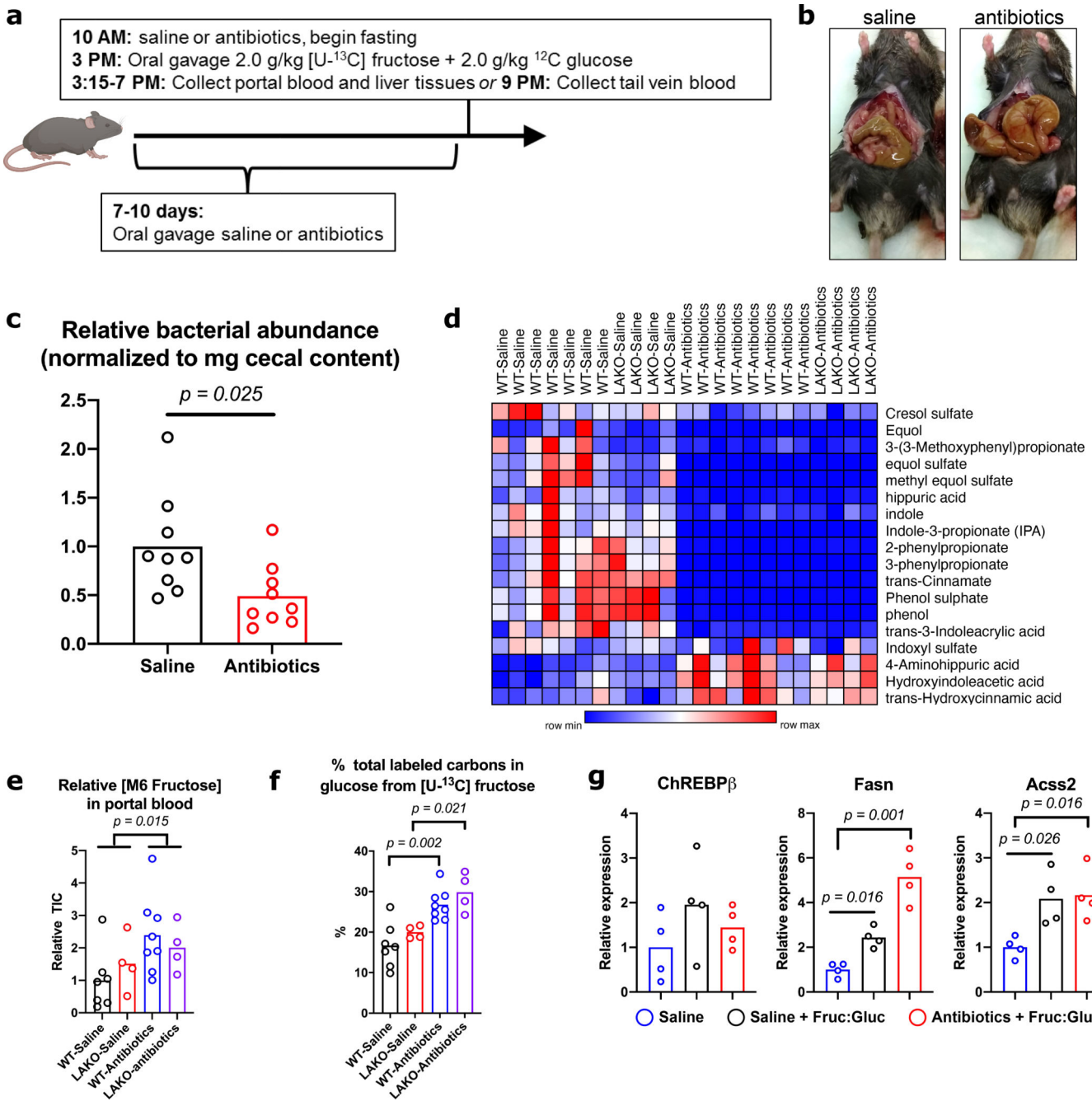

Extended Data Figure 6. Depletion of microbiome blocks substrate contribution, but not signaling component, of de novo lipogenesis following fructose consumption.

a, Experimental set-up for antibiotic depletion of the microbiome followed by ^{13}C-fructose tracing into DNL. **b**, Representative images of cecums from a saline and antibiotic treated mouse. **c**, Relative abundance of bacterial abundance in cecal contents from mice treated with saline (n = 9) or antibiotics (n = 9) as determined by 16s RT-qPCR to a reference standard of E. coli DNA. *P* value determined using Welch's t test. **d**, Heat map of microbial metabolite abundance in the portal blood, collected 1 hour after gavage. **e**, Relative abundance of portal blood ^{13}C-fructose in WT – saline (n = 7) vs. WT – Antibiotics (n = 7)

and LAKO – saline (n = 4) vs. LAKO – antibiotics (n = 4) following gavage and **f**, % total labeled carbons in portal blood glucose, *p* values determined using Welch's t test. **g**, mRNA expression of ChREBPβ, Acss2, and Fasn in liver collected 1 hour after gavage (n = 4/group), *p* values determined using two-sided t tests with Holm-Sidak method for multiple comparisons. For **c**, **e-g**, bars represent mean.

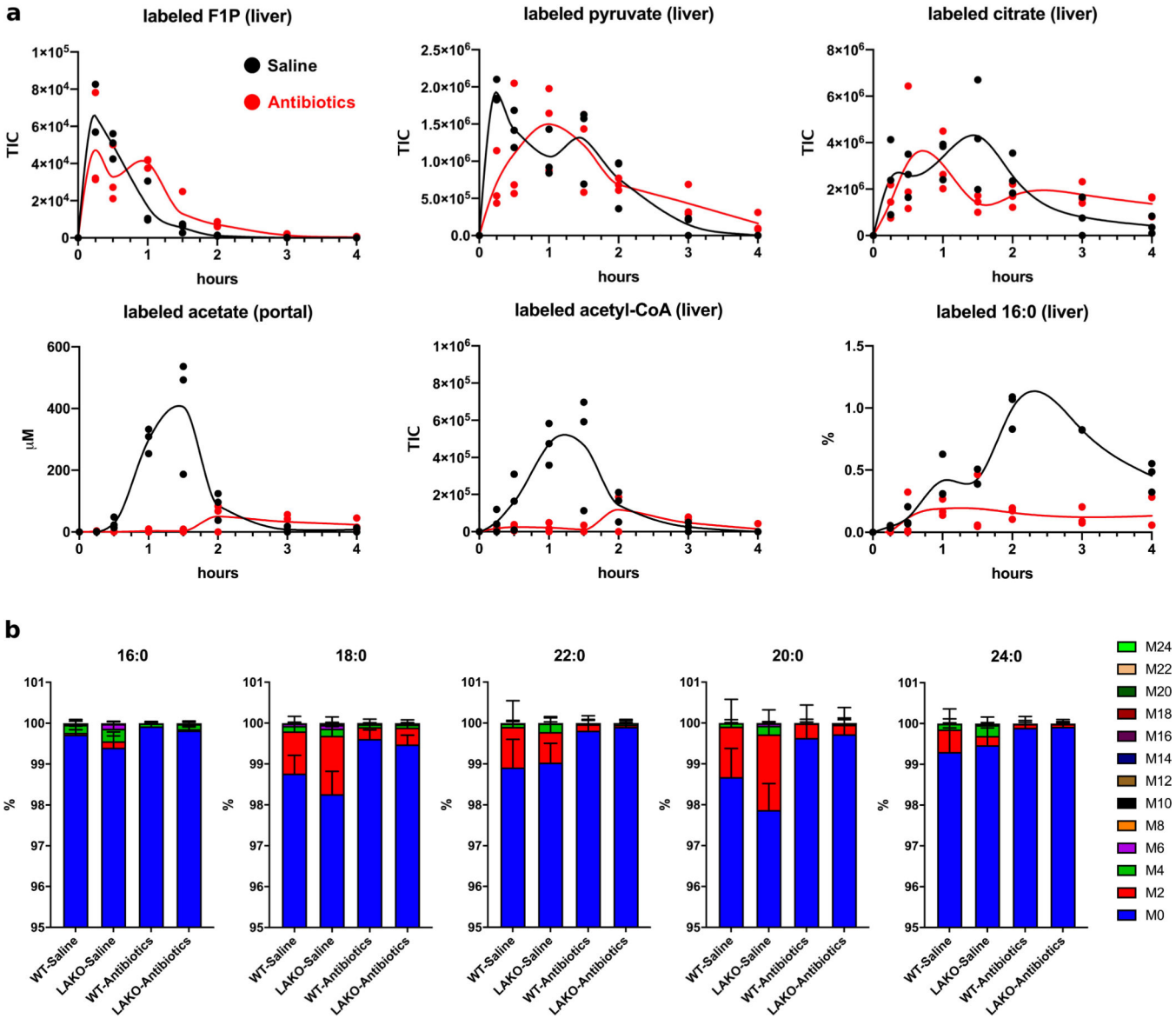

Extended Data Figure 7. Bolus fructose is converted into acetate in a microbiome-dependent manner.

a, TIC of labeled liver F1P, pyruvate, and acetyl-CoA, concentrations (μM) of portal blood labeled acetate, and % labeling of liver saponified 16:0 and 18:0 in saline- or antibiotic-treated WT mice gavaged with 2.0 g/kg ^{13}C-fructose + 2.0 g/kg unlabeled glucose, n = 3 mice/time point. Data for saline-treated mice is also shown in Figure 2d. **b**, Isotopologue distribution of serum saponified fatty acids, collected 6 hours after gavage, data are mean ± SD, n = (WT-Saline: 8, LAKO-Saline: 4, WT-Antibiotics: 8, LAKO-Antibiotics: 4).

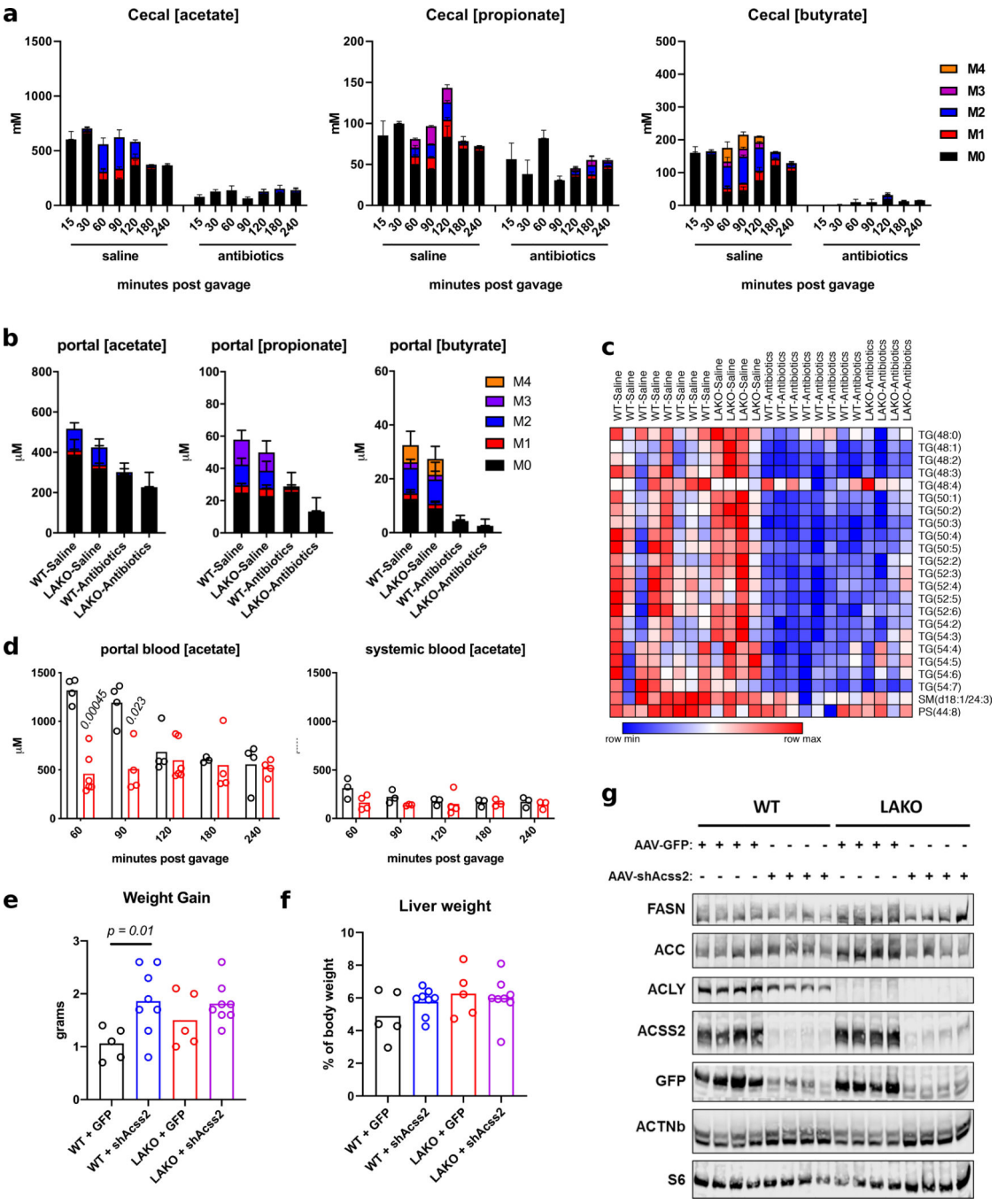

Extended Data Figure 8. Bolus fructose-dependent DNL requires microbial acetate and hepatic ACSS2.

a, Concentrations (μM) of portal blood labeled acetate, propionate, and butyrate, n = (WT-Saline: 8, LAKO-Saline: 4, WT-Antibiotics: 8, LAKO-Antibiotics: 4). **b**, Abundance of cecal labeled acetate, propionate, and butyrate in WT mice, n = 3 mice/timepoint, except for saline-180 n = 2 mice. **c**, Heat map of hepatic triglyceride abundance in livers of saline- or antibiotic-treated mice following an oral gavage of 2.0 g/kg fructose + 2.0 g/kg glucose. **d**, Concentrations of portal and systemic blood acetate following gavage, each data point

represents an individual mouse sacrificed at indicated time, *p* value determined using two-sided t tests with Holm-Sidak method for multiple comparisons. **e**, Weight gain in WT and LAKO mice 1 week following tail-vein injection with AAV8-GFP or AAV8-shAcss2, *p* value determined using Welch's t test. **f**, Liver weight as % of body weight of WT and LAKO mice 1 week following tail-vein injection with AAV8-GFP or AAV8-shAcss2. **g**, Western blot of liver lysates from WT and LAKO mice 1 week following tail-vein injection with AAV8-GFP or AAV8-shAcss2.

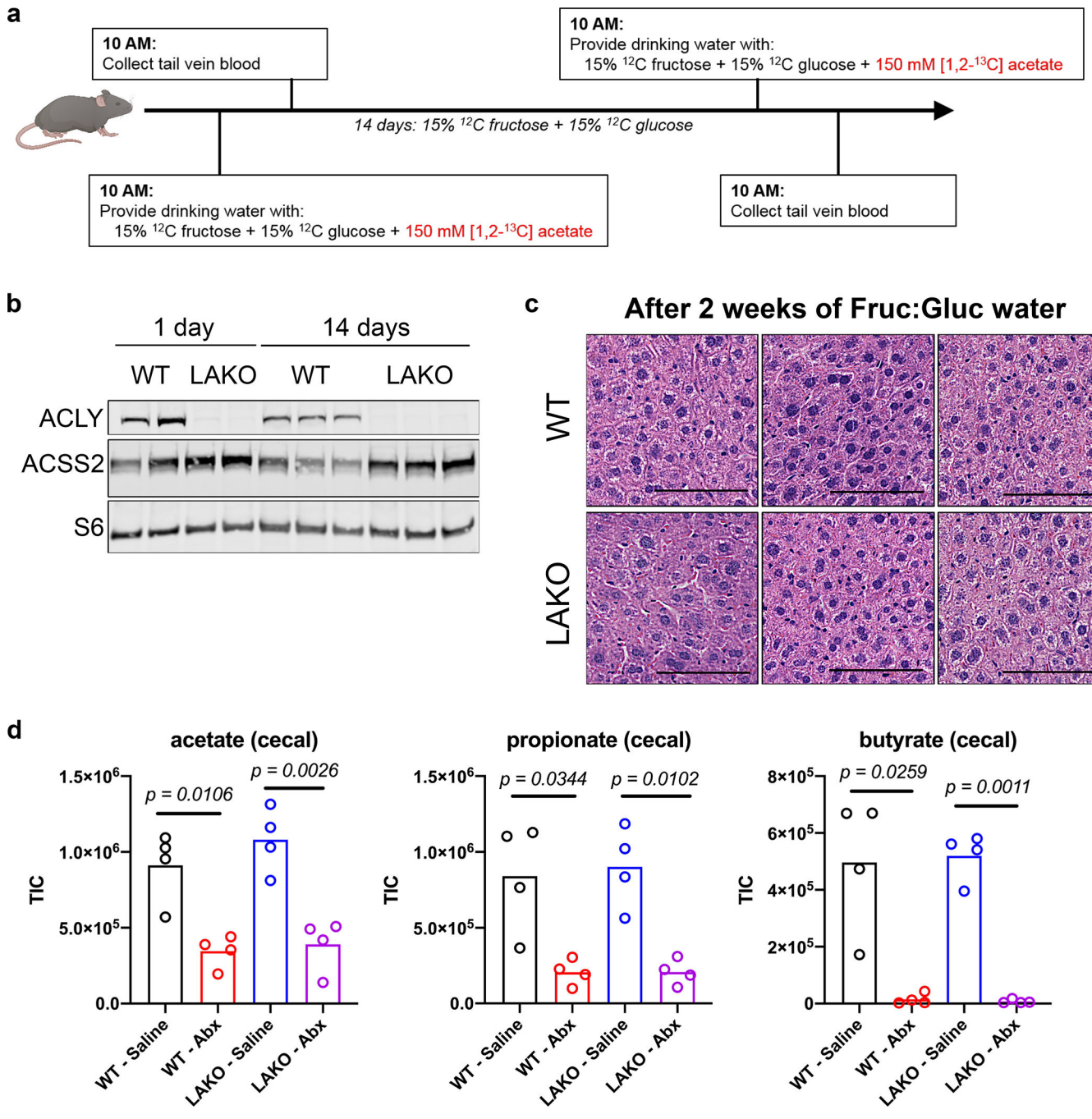

Extended Data Figure 9. Gradual fructose consumption promotes greater acetate usage in LAKO mice.

a, Experimental set-up for ^{13}C-acetate tracing into DNL prior to and after gradual fructose administration. **b**, Western blot of ACLY, ACSS2, and S6 in liver lysates from WT and LAKO mice after 1 day or 14 days of Fruc:Gluc water. **c**, Representative H&E stains of livers from WT and LAKO mice provided Fruc:Gluc water for 2 weeks. Scale bars = 100 μm **d**, Relative abundance of acetate, propionate, and butyrate in the cecal contents of WT and LAKO mice treated with saline or antibiotics for 1 week (n = 4 mice/group). *p* values determined using Welch's t test.

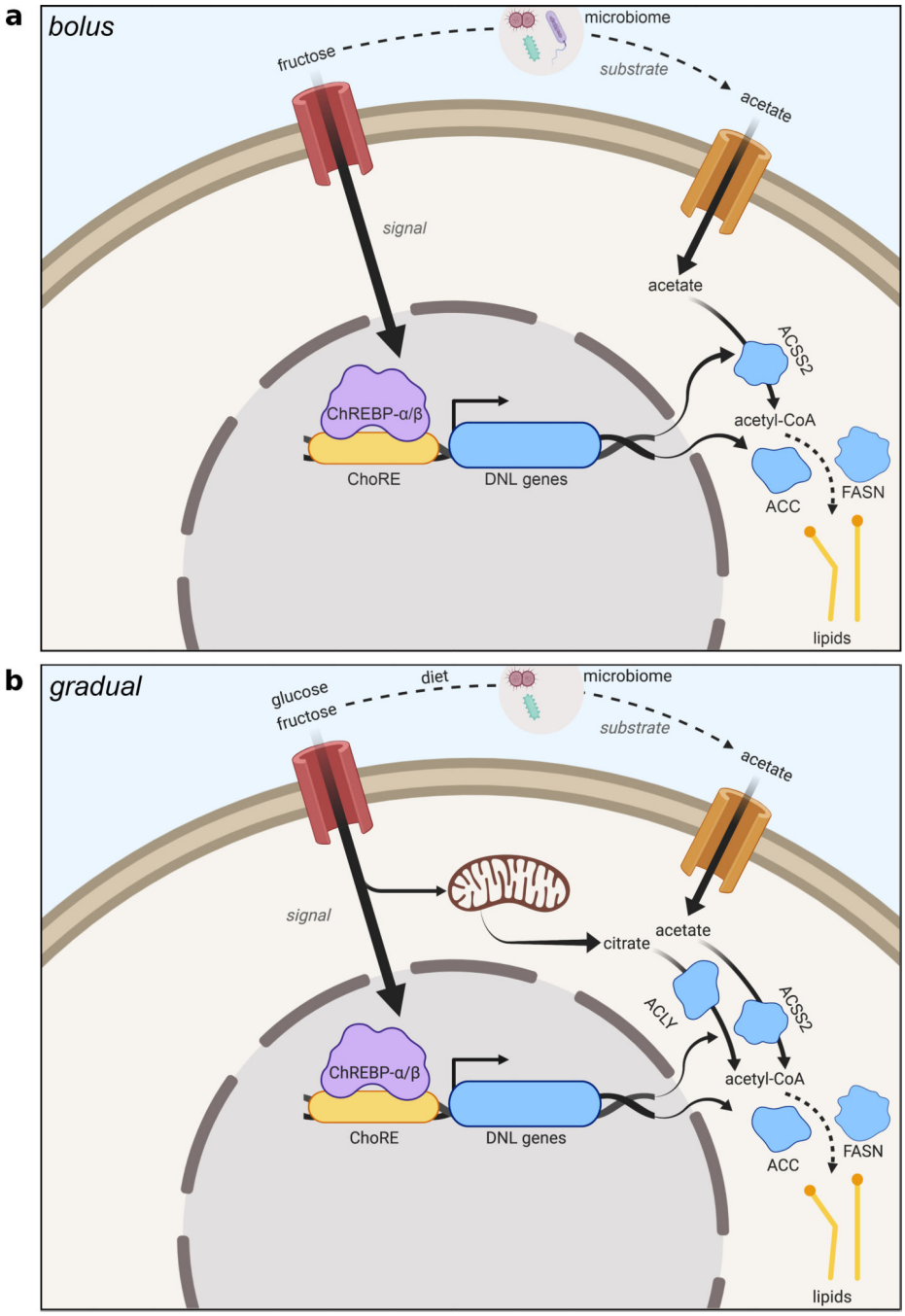

Extended Data Figure 10. Fructose provides signal and substrate to promote hepatic de novo lipogenesis.

a, Proposed model of bolus fructose-induced hepatic DNL. Fructose catabolism in hepatocytes acts as a signal to induce DNL genes including ACSS2, while fructose metabolism by the gut microbiome provides acetate as a substrate to feed DNL, mediated by ACSS2. **b**, Proposed model of gradual fructose-induced hepatic DNL. Like the bolus model, fructose catabolism in hepatocytes acts as a signal to induce DNL genes. Hepatic fructose and glucose (made from fructose by the small intestine) catabolism provide citrate as a

substrate to feed DNL, mediated by ACLY. Metabolism of fibers and other dietary components by the gut microbiome provides acetate as a substrate to feed DNL, following its conversion to acetyl-CoA by hepatic ACSS2. Created with BioRender.com.

Supplementary Material

Refer to Web version on PubMed Central for supplementary material.

Acknowledgements

This work was supported by grant R01CA174761, R01CA228339, and R01DK116005 to K.E.W. S.Z. is supported by pre-doctoral fellowship F99CA222741. C.J. is supported by the American Diabetes Association through post-doctoral fellowship 1-17-PDF-076. K.U. is supported by NIAMS training grant T32AR053461. L.I. is supported by NIGMS training grant T32GM07229. S.T. is supported by the American Diabetes Association through post-doctoral fellowship 1-18-PDF-144. S.F. is supported through the Penn-PORT IRACDA grant K12 GM081259. P.M.T. is supported by K01DK111715. N.W.S. is supported by the NIH grant R03HD092630 and R01GM132261. J.D.R. is supported by the NIH Pioneer Award 1DP1DK113643 and Diabetes Research Center P30 DK019525. We thank Dr. Shelley Berger and Dr. Phillip Mews for providing the AAV.U6.shAcss2.CMV.eGFP.SV40 vector. We thank Dr. Gary Wu and Dr. Yedidya Saimon for helpful discussions on the microbiome.

References

1. Bray GA, Nielsen SJ & Popkin BM Consumption of high-fructose corn syrup in beverages may play a role in the epidemic of obesity. Am. J. Clin. Nutr. 79, 537–43 (2004). [PubMed: 15051594]
2. Jensen T et al. Fructose and sugar: A major mediator of non-alcoholic fatty liver disease. J. Hepatol. 68, 1063–1075 (2018). [PubMed: 29408694]
3. Hannou SA, Haslam DE, McKeown NM & Herman MA Fructose metabolism and metabolic disease. J. Clin. Invest. 128, 545–555 (2018). [PubMed: 29388924]
4. Softic S, Cohen DE & Kahn CR Role of Dietary Fructose and Hepatic De Novo Lipogenesis in Fatty Liver Disease. Dig. Dis. Sci. 61, 1282–1293 (2016). [PubMed: 26856717]
5. Lambert JE, Ramos-Roman MA, Browning JD & Parks EJ Increased de novo lipogenesis is a distinct characteristic of individuals with nonalcoholic fatty liver disease. Gastroenterology 146, 726–735 (2014). [PubMed: 24316260]
6. Donnelly KL et al. Sources of fatty acids stored in liver and secreted via lipoproteins in patients with nonalcoholic fatty liver disease. J. Clin. Invest. 115, 1343–51 (2005). [PubMed: 15864352]
7. Fukuda H, Katsurada A & Iritani N Effects of nutrients and hormones on gene expression of ATP citrate-lyase in rat liver. Eur. J. Biochem. 209, 217–22 (1992). [PubMed: 1396700]
8. Pinkosky SL, Groot PHE, Lalwani ND & Steinberg GR Targeting ATP-Citrate Lyase in Hyperlipidemia and Metabolic Disorders. Trends Mol. Med. 23, 1047–1063 (2017). [PubMed: 28993031]
9. Jang C et al. The Small Intestine Converts Dietary Fructose into Glucose and Organic Acids. Cell Metab. 27, 351–361.e3 (2018). [PubMed: 29414685]
10. Zhao S et al. ATP-Citrate Lyase Controls a Glucose-to-Acetate Metabolic Switch. Cell Rep. 17, 1037–1052 (2016). [PubMed: 27760311]
11. Beigneux AP et al. ATP-citrate lyase deficiency in the mouse. J. Biol. Chem. 279, 9557–64 (2004). [PubMed: 14662765]
12. Herman MA & Samuel VT The Sweet Path to Metabolic Demise: Fructose and Lipid Synthesis. Trends Endocrinol. Metab. 27, 719–730 (2016). [PubMed: 27387598]
13. Uyeda K & Repa JJ Carbohydrate response element binding protein, ChREBP, a transcription factor coupling hepatic glucose utilization and lipid synthesis. Cell Metab. 4, 107–110 (2006). [PubMed: 16890538]
14. Herman MA et al. A novel ChREBP isoform in adipose tissue regulates systemic glucose metabolism. Nature 484, 333–8 (2012). [PubMed: 22466288]

15. Iizuka K The role of carbohydrate response element binding protein in intestinal and hepatic fructose metabolism. Nutrients 9, 1–12 (2017).
16. Poungvarin N et al. Genome-Wide Analysis of ChREBP Binding Sites on Male Mouse Liver and White Adipose Chromatin. Endocrinology 156, 1982–94 (2015). [PubMed: 25751637]
17. Luong A, Hannah VC, Brown MS & Goldstein JL Molecular characterization of human acetyl-CoA synthetase, an enzyme regulated by sterol regulatory element-binding proteins. J. Biol. Chem. 275, 26458–26466 (2000). [PubMed: 10843999]
18. Ikeda Y et al. Transcriptional Regulation of the Murine Acetyl-CoA Synthetase 1 Gene through Multiple Clustered Binding Sites for Sterol Regulatory Element-binding Proteins and a Single Neighboring Site for Sp1. J. Biol. Chem. 276, 34259–34269 (2001). [PubMed: 11435428]
19. Softic S et al. Divergent effects of glucose and fructose on hepatic lipogenesis and insulin signaling. J. Clin. Invest. 127, 4059–4074 (2017). [PubMed: 28972537]
20. Liu X et al. Acetate Production from Glucose and Coupling to Mitochondrial Metabolism in Mammals. Cell 175, 502–513.e13 (2018). [PubMed: 30245009]
21. Bulusu V et al. Acetate Recapturing by Nuclear Acetyl-CoA Synthetase 2 Prevents Loss of Histone Acetylation during Oxygen and Serum Limitation. Cell Rep. 18, 647–658 (2017). [PubMed: 28099844]
22. Lu M et al. ACOT12-Dependent Alteration of Acetyl-CoA Drives Hepatocellular Carcinoma Metastasis by Epigenetic Induction of Epithelial-Mesenchymal Transition. Cell Metab. 1–15 (2019). doi:10.1016/j.cmet.2018.12.019
23. Ter Horst KW & Serlie MJ Fructose consumption, lipogenesis, and non-alcoholic fatty liver disease. Nutrients 9, 1–20 (2017).
24. Bergheim I et al. Antibiotics protect against fructose-induced hepatic lipid accumulation in mice: Role of endotoxin. J. Hepatol. 48, 983–992 (2008). [PubMed: 18395289]
25. Kaden-Volynets V et al. Lack of liver steatosis in germ-free mice following hypercaloric diets. Eur. J. Nutr. 0, 1–13 (2018).
26. Mews P et al. Acetyl-CoA synthetase regulates histone acetylation and hippocampal memory. Nature 546, 381–386 (2017). [PubMed: 28562591]
27. Li MV et al. Glucose-6-phosphate mediates activation of the carbohydrate responsive binding protein (ChREBP). Biochem. Biophys. Res. Commun. 395, 395–400 (2010). [PubMed: 20382127]
28. Lanaspa MA et al. Ketohexokinase C blockade ameliorates fructose-induced metabolic dysfunction in fructose-sensitive mice. J. Clin. Invest. 128, 2226–2238 (2018). [PubMed: 29533924]
29. Ishimoto T et al. Opposing effects of fructokinase C and A isoforms on fructose-induced metabolic syndrome in mice. Proc. Natl. Acad. Sci. U. S. A. 109, 4320–5 (2012). [PubMed: 22371574]
30. Parks EJ, Skokan LE, Timlin MT & Dingfelder CS Dietary Sugars Stimulate Fatty Acid Synthesis in Adults. J. Nutr. 1039–1046 (2008). doi:10.1016/j.bbi.2008.05.010 [PubMed: 18492831]
31. den Besten G et al. Gut-derived short-chain fatty acids are vividly assimilated into host carbohydrates and lipids. Am. J. Physiol. - Gastrointest. Liver Physiol. 305, 900–910 (2013).
32. Donohoe DR et al. The Warburg Effect Dictates the Mechanism of Butyrate-Mediated Histone Acetylation and Cell Proliferation. Mol. Cell 48, 612–626 (2012). [PubMed: 23063526]
33. Zagelbaum NK, Yandrapalli S, Nabors C & Frishman WH Bempedoic Acid (ETC-1002): ATP Citrate Lyase Inhibitor: Review of a First-in-Class Medication with Potential Benefit in Statin-Refractory Cases. Cardiol. Rev. 27, 49–56 (2018).
34. Guo L et al. Enhanced acetylation of ATP-citrate lyase promotes the progression of nonalcoholic fatty liver disease. J. Biol. Chem. 294, 11805–11816 (2019). [PubMed: 31197036]
35. Wang Q et al. Abrogation of hepatic ATP-citrate lyase protects against fatty liver and ameliorates hyperglycemia in leptin receptor-deficient mice. Hepatology 49, 1166–75 (2009). [PubMed: 19177596]
36. Wang Q et al. Deficiency in hepatic ATP-citrate lyase affects VLDL-triglyceride mobilization and liver fatty acid composition in mice. J. Lipid Res. 51, 2516–26 (2010). [PubMed: 20488800]

Method References

37. Postic C et al. Dual roles for glucokinase in glucose homeostasis as determined by liver and pancreatic b cell-specific gene knock-outs using Cre recombinase. J. Biol. Chem. 274, 305–315 (1999). [PubMed: 9867845]
38. Nadkarni MA, Martin FE, Jacques NA & Hunter N Determination of bacterial load by real-time PCR using a broad-range (universal) probe and primers set. Microbiology 148, 257–266 (2002). [PubMed: 11782518]
39. Guan D et al. Diet-Induced Circadian Enhancer Remodeling Synchronizes Opposing Hepatic Lipid Metabolic Processes. Cell 174, 831–842.e12 (2018). [PubMed: 30057115]
40. Su X, Lu W & Rabinowitz JD Metabolite Spectral Accuracy on Orbitraps. Anal. Chem. 89, 5940–5948 (2017). [PubMed: 28471646]
41. Titchenell PM, Chu Q, Monks BR & Birnbaum MJ Hepatic insulin signalling is dispensable for suppression of glucose output by insulin in vivo. Nat. Commun. 6, 1–9 (2015).
42. Iroz A et al. A Specific ChREBP and PPARα Cross-Talk Is Required for the Glucose-Mediated FGF21 Response. Cell Rep. 21, 403–416 (2017). [PubMed: 29020627]
43. Frey AJ et al. LC-quadrupole/Orbitrap high-resolution mass spectrometry enables stable isotope-resolved simultaneous quantification and 13C-isotopic labeling of acyl-coenzyme A thioesters. Anal. Bioanal. Chem. 408, 3651–3658 (2016). [PubMed: 26968563]
44. Trefely S, Ashwell P & Snyder NW FluxFix: automatic isotopologue normalization for metabolic tracer analysis. BMC Bioinformatics 17, 485 (2016). [PubMed: 27887574]
45. Lee JV et al. Acetyl-CoA promotes glioblastoma cell adhesion and migration through Ca2+-NFAT signaling. Genes Dev. 32, (2018).
46. Chong J et al. MetaboAnalyst 4.0: towards more transparent and integrative metabolomics analysis. Nucleic Acids Res. 46, W486–W494 (2018). [PubMed: 29762782]
47. Neinast MD et al. Quantitative Analysis of the Whole-Body Metabolic Fate of Branched-Chain Amino Acids. Cell Metab. 1–13 (2018). doi:10.1016/j.cmet.2018.10.013

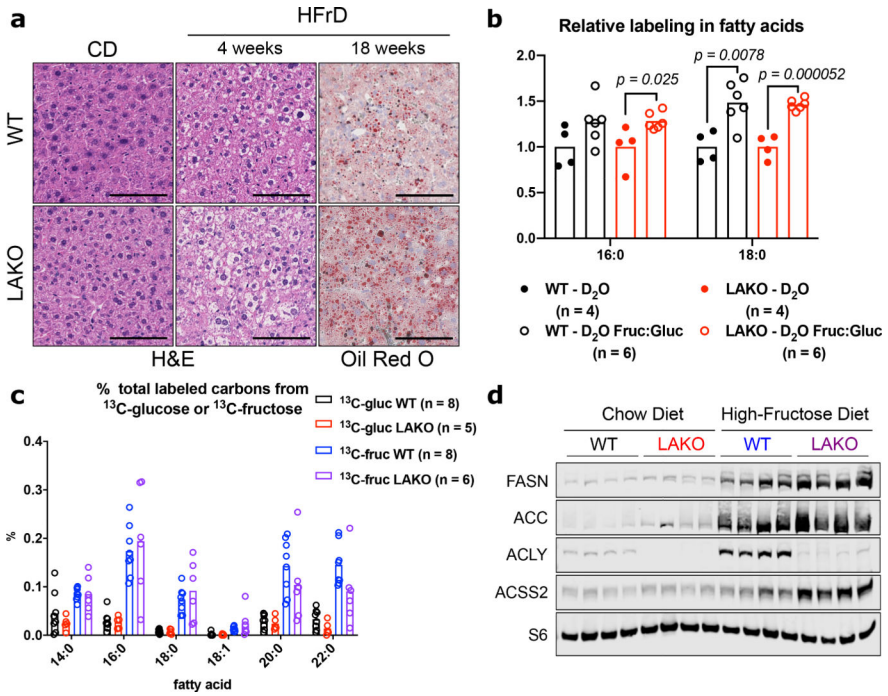

Figure 1. Fructose-dependent fatty acid synthesis is ACLY-independent.

a, Representative H&E and Oil Red O histological stains of livers of WT or LAKO mice on chow (CD) or high fructose diet (HFrD) from two independent experiments of n = 4 WT and LAKO mice/diet (4 weeks) and n = 13 WT mice/diet and n = 6 LAKO mice/diet (18 weeks). Scale bars = 100 μm. **b**, Relative deuterium incorporation in palmitic acid (16:0) and stearic acid (18:0) after 24 hour D_2O labeling of mice, D_2O set to 1 and compared to D_2O Fruc:Gluc within each genotype, significance determined by two-sided t tests. **c**, % total labeled carbons in serum saponified fatty acids from mice gavaged with 1:1 fructose:glucose, ^{13}C-labeled substrate indicated, bars represent mean. **d**, Immunoblots of lipogenic enzymes in livers of WT or LAKO mice fed CD or HFrD for 4 weeks.

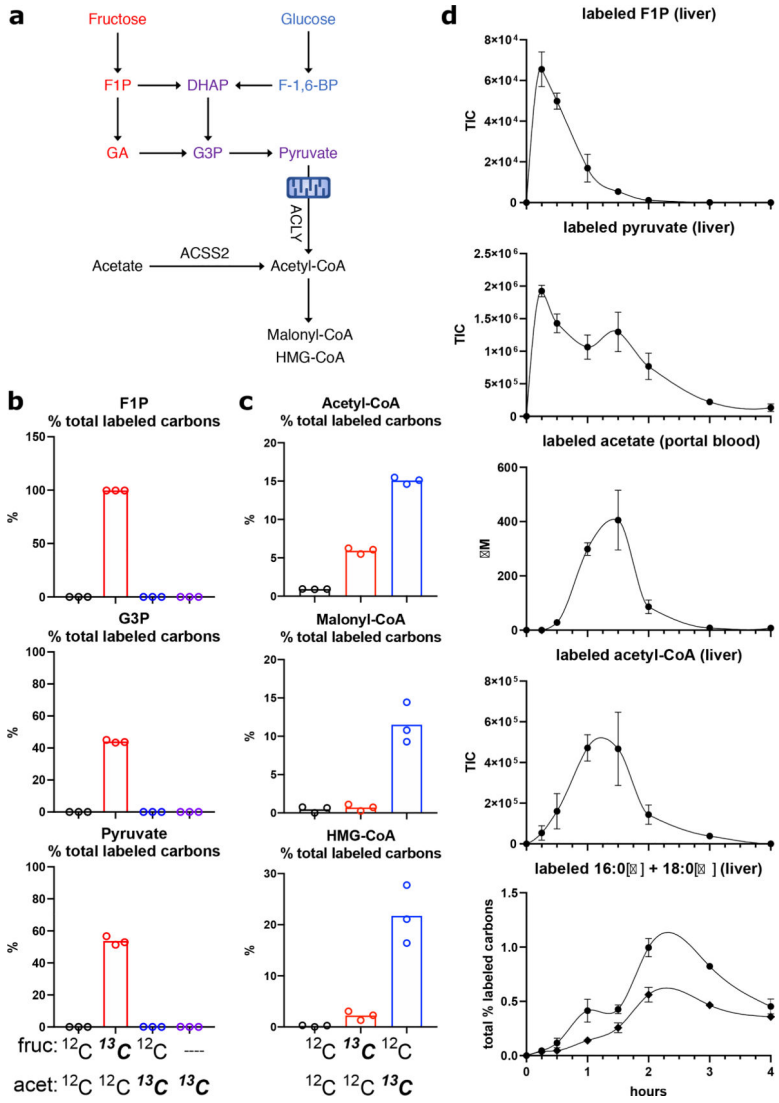

Figure 2. Lipogenic acetyl-CoA is preferentially produced from acetate in hepatocytes.

a, Pathways for lipogenic acetyl-CoA production from fructose, glucose, or acetate. **b-c**, % total labeled carbons in fructolytic intermediates (**b**) and acetyl-CoA, malonyl-CoA, or HMG-CoA (**c**) in primary hepatocytes incubated for 6 hours with 25mM fructose + 1mM acetate, ^{13}C-labeled substrate indicated, bars represent mean, n = 3. **d**, Total ion counts (TIC) of labeled liver F1P, pyruvate, and acetyl-CoA, concentrations (μM) of portal blood labeled acetate, and % labeling of liver 16:0 and 18:0 in saline-treated WT mice gavaged with 1:1 ^{13}C-fructose:glucose, data are mean ± SEM, n = 3 mice/time point.

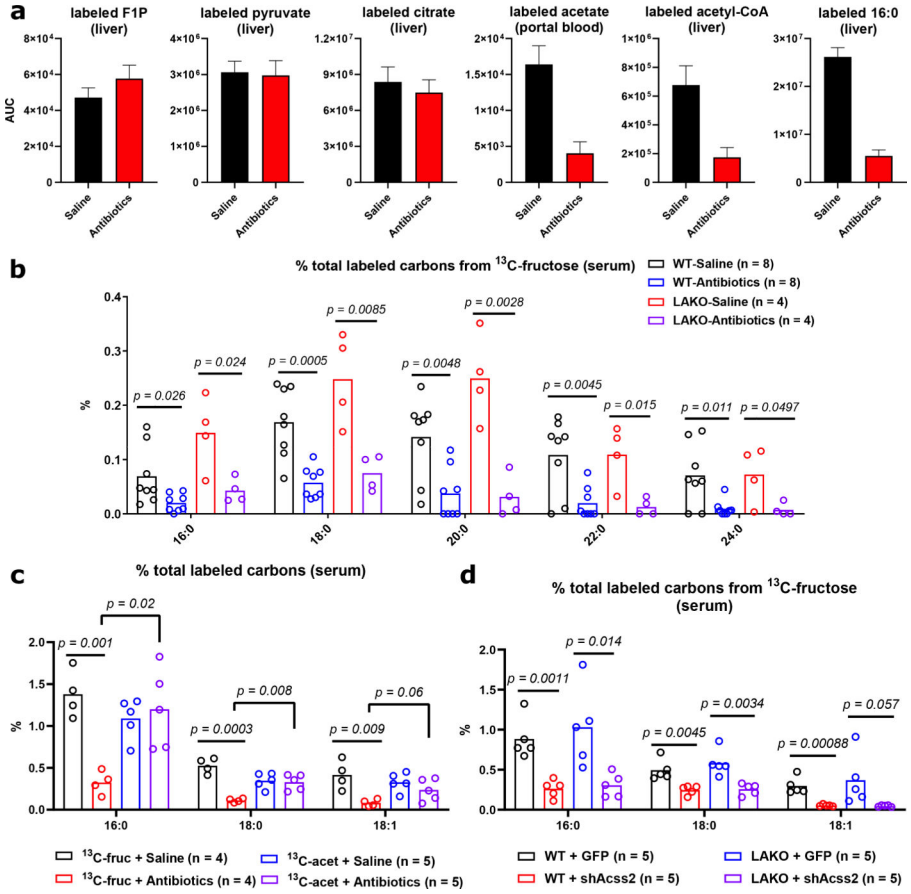

Figure 3. Metabolism of bolus fructose by the microbiome feeds hepatic lipogenesis.

a, Area under curve ($AUC_{0–240}$ min) of labeled hepatic F1P, pyruvate, acetyl-CoA, palmitate and portal blood acetate, data are mean ± SEM. See Extended Data Figure 8a for curves. **b**, % total labeled carbons in serum saponified fatty acids from saline- or antibiotic-treated LAKO mice gavaged with ^{13}C-fructose:glucose, significance determined using two-sided t tests. **c**, % total labeled carbons in serum saponified fatty acids from saline- or antibiotic-treated LAKO mice gavaged with 1:1 fructose:glucose + 0.5 g/kg acetate, ^{13}C-labeled substrate indicated, significance determined by two-sided t test. **d**, % total labeled carbons in serum saponified fatty acids from WT and LAKO mice 1 week after injection with AAV-GFP or AAV-shAcss2, significance determined by two-sided t test. For **b-c**, bars represent mean.

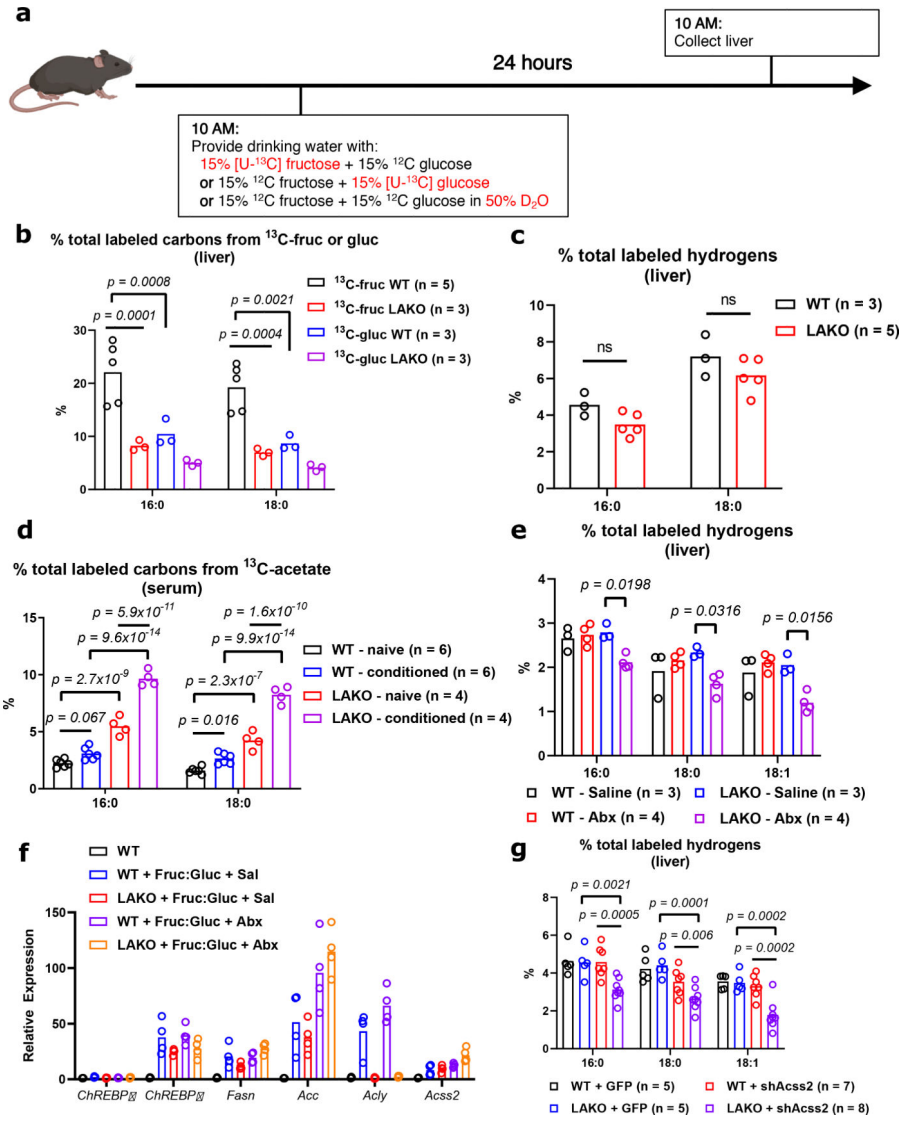

Figure 4. Gradual fructose consumption promotes hepatic lipogenesis from ACLY- and ACSS2-derived acetyl-CoA.

a, Experimental design for gradual fructose consumption. **b**, % total labeled carbons from ^{13}C-fructose or glucose in hepatic saponified fatty acids, WT vs. LAKO. **c**, % total labeled hydrogens from D_2O in hepatic saponified fatty acids. **d**, % total labeled carbons from ^{13}C-acetate in serum saponified fatty acids, see Extended Data Fig. 10a for experimental design. **e**, total % labeled hydrogens from D_2O in hepatic saponified fatty acids in WT and LAKO mice following 1 week treatment with saline or antibiotics (abx). **f**, mRNA expression of ChREBP and lipogenic genes in livers of mice in (**e**). **g**, total % hydrogens labeled in hepatic saponified fatty acids in WT and LAKO mice 1 week after injection with AAV-GFP or AAV-shAcss2. For **b-g**, bars represent mean, **b-e,g**, significance determined using 2-way ANOVA with Tukey's test for multiple comparisons.